

# Inclusions, Boundaries and Disorder in Scalar Active Matter

Omer Granek and Yariv Kafri

*Department of Physics,  
Technion – Israel Institute of Technology, Haifa 32000,  
Israel*

Mehran Kardar, Sunghan Ro, and Julien Tailleur

*Department of Physics,  
Massachusetts Institute of Technology,  
Cambridge, Massachusetts 02139,  
USA*

Alexandre Solon

*Sorbonne Université, CNRS,  
Laboratoire de Physique Théorique de la  
Matière Condensée (UMR CNRS 7600),  
4 Place Jussieu,  
75252 Paris Cedex 05,  
France*

Active systems are driven out of equilibrium by exchanging energy and momentum with their environment. This endows them with anomalous mechanical properties that we review in this colloquium for the case of dry scalar active matter, which has attracted considerable attention. These unusual properties lead to a rich physics when active fluids are in contact with boundaries, inclusions, tracers, or disordered potentials. Indeed, studies of the mechanical pressure of active fluids and of the dynamics of passive tracers have shown that active systems impact their environment in non-trivial ways, for example, by propelling and rotating anisotropic inclusions. Conversely, the long-ranged density and current modulations induced by localized obstacles show how the environment can have a far-reaching impact on active fluids. This is best exemplified by the propensity of bulk and boundary disorder to destroy bulk phase separation in active matter, showing active systems to be much more sensitive to their surroundings than passive ones. This colloquium aims at providing a unifying perspective on the rich interplay between active systems and their environments.

## CONTENTS

I. Introduction	1	A. A simple physical picture	17
II. Scalar Active Matter	2	B. Field-theoretical description	18
A. Noninteracting active particles	2	VI. Boundary disorder.	20
B. Interacting scalar active matter	3	A. A simple physical picture	20
C. Collective behavior	4	B. Linear field theory	21
1. Bulk phase separation in scalar active matter	4	C. The effect of disordered boundaries on MIPS	22
2. A minimal hydrodynamic description of MIPS	5	VII. Conclusion, perspectives.	22
3. Beyond the simple MIPS scenario	5	Acknowledgments	22
III. Mechanical forces on confining boundaries	6	References	23
A. Mechanical pressure on flat confining boundaries	7		
B. Curved and flexible boundaries	9		
IV. Obstacles and localized inclusions	11		
A. A single obstacle in an infinite system	12		
B. Finite systems and boundary conditions	12		
C. Non-reciprocal mediated interactions.	13		
D. Mobile obstacles and dynamics	13		
1. Phenomenological description of symmetric tracers	14		
2. The Markovian approximation	14		
3. Beyond the Markovian approximation	15		
E. Coupled dynamics of passive tracers: Non-reciprocal interactions and localization	16		
V. Bulk disorder	16		

## I. INTRODUCTION

Active matter comprises entities that dissipate energy to exert propelling forces on their environment (Bechinger *et al.*, 2016; Chaté, 2020; Fodor and Marchetti, 2018; Marchetti *et al.*, 2013; Ramaswamy, 2010; Tailleur *et al.*, 2022). From molecular motors to bacteria and large groups of animals, active systems are ubiquitous in biology. Furthermore, over the past two decades, physicists and chemists have devised active particles in the lab, paving the way toward engineering syn-

thetic active materials. The non-equilibrium drive at the microscopic scale endows active materials with a plethora of collective behaviors unmatched in equilibrium physics. The rich contrast with equilibrium has germinated considerable experimental and theoretical research on the subject, which has turned *active matter* into a central field of condensed matter physics.

One of the most striking differences between active and passive systems lies in their manifestations of force and work, running counter to intuition from equilibrium thermodynamics. While in some aspects, bulk fluids of active particles resemble equilibrium matter, the forces exerted on their confining vessels (Junot *et al.*, 2017; Solon *et al.*, 2015b; Takatori *et al.*, 2014; Yang *et al.*, 2014; Zakine *et al.*, 2020) display a host of unusual phenomena. Examples range from ratchet currents (Di Leonardo *et al.*, 2010; Sokolov *et al.*, 2010), to anisotropic pressure (Solon *et al.*, 2015b), and long-ranged density modulations induced by inclusions (Angelani *et al.*, 2011; Baek *et al.*, 2018; Galajda *et al.*, 2007; Rodenburg *et al.*, 2018; Tailleur and Cates, 2009). More recently, it became clear that the set of results pertaining to boundaries, inclusions and tracers, and to the forces exerted on them, have a much broader impact in the context of disordered active materials (Chardac *et al.*, 2021; Duan *et al.*, 2021; Morin *et al.*, 2017; Toner *et al.*, 2018). In particular, disorder has been shown to play a fundamentally different role for active systems than for equilibrium ones (Ben Dor *et al.*, 2022b, 2019; Ro *et al.*, 2021).

In this colloquium, we review recent results on scalar active matter in the presence of boundaries, inclusions, tracers, and disorder, for which we try to offer a coherent physical picture. Scalar systems correspond to ‘dry’ active matter whose only hydrodynamic mode is the conserved density field. It offers the simplest-yet-not-too-simple framework to study the interplay between activity and mechanical forces. The insights gained from studying these systems can then be used in other situations, such as ‘wet’ active matter, where the presence of a momentum-conserving solvent plays an important role. Similarly, the interplay between activity and mechanics in polar or nematic active fluids forms a current frontier of the field that is beyond the scope of this colloquium.

We first briefly introduce scalar active matter in Sec. II, starting at the single-particle level and progressing to collective behaviors. Then, in Sec. III we discuss the anomalous properties of the forces that active fluids exert on confining boundaries. In Sec. IV, we turn to obstacles and tracers immersed in active baths. The results presented in these sections finally allow us to discuss the effect of bulk and boundary disorder on active fluids in Secs. V and VI, respectively.

## II. SCALAR ACTIVE MATTER

To introduce scalar active matter at the microscopic scale, we first review the standard models of active particles in Sec. II.A. We then discuss in Sec. II.B the different interactions between particles that have been considered, and the conditions under which the resulting large-scale physics reduces to the dynamics of a single density field. Finally, we describe the collective behaviors encountered in scalar active systems in Sec. II.C, focusing on Motility-Induced Phase Separation (MIPS), and we review the corresponding hydrodynamic description in Sec. II.C.2.

### A. Noninteracting active particles

A large diversity of active particles, each capable of dissipating energy to self-propel, exists across scales in nature, from molecular motors at the nano-scale to cells and macroscopic animals. In addition, many types of artificial self-propelled particles (SPPs) are now engineered, examples being chemically powered Janus colloids (Howse *et al.*, 2007), colloidal rollers (Bricard *et al.*, 2013), vibrated grains (Deseigne *et al.*, 2010), self-propelled droplets (Thutupalli *et al.*, 2011) or ‘hexbug’ toy robots (Li and Zhang, 2013), to name but a few. Although they vary greatly in their details, these active particles share the feature of being persistent random walkers. Compared to a passive random walker, this introduces a typical scale separating ballistic motion at a small scale from a diffusive behavior on large scales. This scale is quantified by the persistence time  $\tau$  and the average distance traveled during this time, which is called the persistence length  $\ell_p$ . Three types of active particles have been most commonly used in theoretical and numerical studies of active matter.

Active Brownian particles (ABPs) (Fily and Marchetti, 2012) and run-and-tumble particles (RTPs) (Schnitzer, 1993) propel at a constant speed  $v_p = \mu f_p$ , where  $\mu$  is the particle mobility and  $f_p$  is the constant magnitude of the self-propelling force. The orientations of ABPs change continuously due to rotational diffusion, characterized by a rotational diffusivity  $D_r$ . By contrast, RTPs randomize their directions of motion instantaneously during ‘tumbles’ that occur at a constant rate  $\alpha$ . ABPs are a good model for self-propelled colloids (Ginot *et al.*, 2018; Howse *et al.*, 2007), while RTPs have been used to model the dynamics of swimming bacteria like E.Coli (Berg, 2004). The spatial dynamics of RTPs and ABPs, in their simplest form, reads

$$\dot{\mathbf{r}}(t) = \mu \mathbf{f}_p(t), \quad (1)$$

where the self-propulsion force  $\mathbf{f}_p(t)$  can be seen as a non-Gaussian noise of fixed magnitude  $f_p$ . The persistence time of an ABP in  $d$  space dimensions is  $\tau =$

$[(d-1)D_\tau]^{-1}$  while  $\tau = \alpha^{-1}$  for RTPs. The corresponding persistence length is given by  $\ell_p = \mu f_p \tau$ .

To model active particles whose propulsion forces have fluctuating norms, a third model has been introduced in which the active force evolves according to an Ornstein-Uhlenbeck process:

$$\tau \dot{\mathbf{f}}_p = -\mathbf{f}_p + \frac{\sqrt{2D_{\text{eff}}}}{\mu} \boldsymbol{\eta}. \quad (2)$$

Here,  $\boldsymbol{\eta}(t)$  is a centered Gaussian white noise of unit amplitude and independent components. This model is commonly referred to as Active Ornstein-Uhlenbeck particles (AOUPs). It was studied long before active matter existed as a field, as one of the simplest models of diffusion with colored noise (Hänggi and Jung, 1994). In the context of active matter, AOUPs were independently introduced to model the dynamics of crawling cells (Sepúlveda *et al.*, 2013) and as a simplified model for which analytical progress is tractable (Szamel, 2014)<sup>1</sup>. The Gaussian nature of the self-propelled force has indeed allowed studying analytically a variety of problems (Berthier *et al.*, 2017; Fodor *et al.*, 2016; Maggi *et al.*, 2015; Martin *et al.*, 2021; Wittmann *et al.*, 2017a,b; Woillez *et al.*, 2020a,b). For AOUPs, the persistence time is given by  $\tau$ , while the typical propulsion force can be defined from  $f_p^2 = \langle \mathbf{f}_p^2 \rangle = dD_{\text{eff}}/(\mu^2\tau)$ , where  $\langle \cdot \rangle$  is an average over histories. The persistence length can then be computed as

$$\ell_p \equiv \left\langle \frac{[\mathbf{r}(t) - \mathbf{r}(0)] \cdot \mathbf{f}_p(0)}{|\mathbf{f}_p(0)|} \right\rangle_{t \rightarrow \infty} \sim \mu\tau \langle |\mathbf{f}_p(0)| \rangle = \sqrt{\frac{2D_{\text{eff}}\tau}{\pi}}.$$

Despite their different dynamics, ABPs, RTPs and AOUPs all lead to force auto-correlation functions that decay exponentially in time:

$$\langle f_{p,i}(t) f_{p,j}(0) \rangle = \delta_{ij} \frac{f_p^2}{d} e^{-t/\tau}, \quad (3)$$

with  $f_{p,k}$  denoting the spatial components of  $\mathbf{f}_p$ . At large scales, all lead to diffusive dynamics with an effective diffusion coefficient  $D_{\text{eff}} = \mu^2 f_p^2 \tau / d$ . For ABPs and RTPs, this can be written as  $D_{\text{eff}} = \ell_p^2 / (d\tau)$ . For AOUPs, the scale of the active force is proportional to the number of space dimensions and the fluctuations of  $f_p$  lead to an extra contribution to the diffusivity, so that  $D_{\text{eff}} = \pi \ell_p^2 / (2\tau)$ .

Typical trajectories for the three types of particles are shown in Fig. 1 (top), which highlights their differences on short length scales. While these differences are irrelevant at the scale of diffusive dynamics, they play

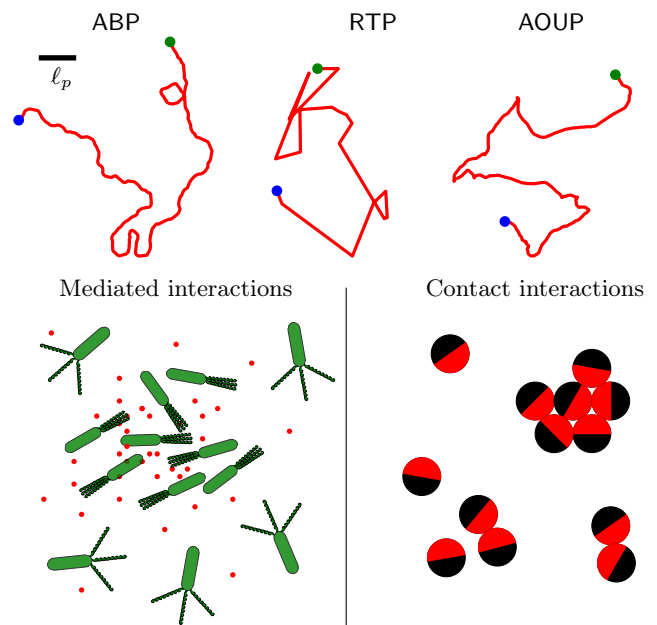


FIG. 1 **Top**: Representative trajectories for the three types of active particles described in Sec. II.A, all with the same persistence time  $\tau = 1$ , total duration  $T = 20$  and effective diffusion coefficient  $D_{\text{eff}} = 1$ . This corresponds to  $v_p = \sqrt{2}$  (for ABP and RTP) and a persistence length  $\ell_p = \sqrt{2}$  indicated as a scale bar. The blue and green dots indicate the starting and finishing positions, respectively. **Bottom**: Schematic representation of mediated and contact interactions occurring between active particles.

an important role in the presence of external potentials. For example, in the large persistence regime, it has been predicted theoretically (Basu *et al.*, 2020; Hennes *et al.*, 2014; Malakar *et al.*, 2020; Smith *et al.*, 2022; Solon *et al.*, 2015a; Tailleur and Cates, 2008, 2009) and observed experimentally (Schmidt *et al.*, 2021; Takatori *et al.*, 2016) that RTPs and ABPs accumulate away from the center of a confining harmonic well. On the contrary, in a harmonic potential, AOUPs always have a steady state given by a centered Gaussian distribution (Szamel, 2014) and, somewhat surprisingly, their dynamics obey detailed balance (Fodor *et al.*, 2016).

## B. Interacting scalar active matter

In this colloquium, we focus on scalar active matter, i.e., on active systems whose long-time and large-scale behaviors are entirely captured by the stochastic dynamics of a density field. All dilute dry active systems fall in this class, as do a wealth of interacting ones.

A scalar theory generically describes systems where the interactions only depend on and impact the particle positions. This is for instance the case for attractive or repulsive pairwise forces that play an important role in

<sup>1</sup> Other models of active particles have also been considered in the literature, e.g. by considering underdamped Langevin equations with nonlinear friction (Romanczuk *et al.*, 2012). In some limits, they yield back the standard ABP and RTP models.

dense active systems (Fily and Marchetti, 2012; Redner *et al.*, 2013b; Stenhammar *et al.*, 2014, 2015; Wysocki *et al.*, 2014). It also applies to interactions that act only on the magnitude of the self-propulsion velocity and not on its direction (D’Alessandro *et al.*, 2017; Liu *et al.*, 2011). Such interactions can, for instance, be mediated by chemical signals as encountered in assemblies of cells interacting via “quorum sensing” (QS). This is depicted in Fig. 1 (bottom left) where the cells adapt their behaviors to the concentration of diffusing signaling molecules. QS is generic in nature (Miller and Bassler, 2001) and plays an important role in diverse biological functions ranging from bioluminescence (Engebrecht and Silverman, 1984; Fuqua *et al.*, 1994; Nealson *et al.*, 1970; Verma and Miyashiro, 2013) and virulence (Tsou and Zhu, 2010) to biofilm formation and swarming (Daniels *et al.*, 2004; Hamner and Bassler, 2003). It can also be engineered by genetic manipulation of bacteria (Curatolo *et al.*, 2020; Liu *et al.*, 2011) or using light-controlled colloids (Bauerle *et al.*, 2018; Massana-Cid *et al.*, 2022). Integrating out the dynamics of the mediating chemical field, particles interacting via QS can be modeled by motility parameters that depend on the density field, for example, through a density-dependent self-propulsion force  $f_p(\mathbf{r}, [\rho])$  (Cates and Tailleur, 2015).

It is important to note that many active systems also experience interactions that require more complex effective (‘hydrodynamic’) descriptions. This is, for example, the case when the rotational symmetry of the system is spontaneously broken. The prototypical example is that of the Vicsek model (Vicsek *et al.*, 1995) where strong-enough aligning torques between the particles lead to the emergence of an ordered polar phase in dense systems (Chate, 2020; Marchetti *et al.*, 2013). A proper hydrodynamic description of the corresponding flocking phase then requires the inclusion of the orientation field (Toner *et al.*, 2005). A wealth of other interactions may impact the particle’s orientations, like chemotaxis (Berg, 2004)—which makes cells move preferably up or down chemical gradients—, or contact inhibition of locomotion (Stramer and Mayor, 2017) that may lead to cells reverting their directions of motion upon encounters. We stress that the disordered phases of all such systems nevertheless remain part of scalar active matter and already exhibit non-trivial collective behaviors (Brenner *et al.*, 1998; O’Byrne and Tailleur, 2020; Saha *et al.*, 2014; Sese-Sansa *et al.*, 2018; Spera *et al.*, 2023).

### C. Collective behavior

In this Section, we turn to the collective behaviors that are typically encountered in scalar active matter.

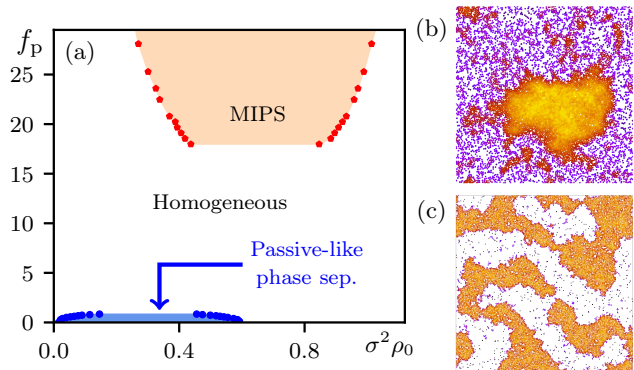


FIG. 2 Simulations of ABPs interacting via a Lennard-Jones potential,  $V(r) = 4\epsilon[(\frac{\sigma}{r})^{12} - (\frac{\sigma}{r})^6]$  for  $r < 2.7\sigma$  and  $V(r) = 0$  otherwise. (a) Phase diagram obtained by varying  $f_p$  and the average density  $\rho_0$ . (b) Representative snapshot of the system in the MIPS region ( $f_p = 42$ ,  $\rho_0 = 0.9$ ). (c) Representative snapshot of the system in the passive-like phase separation, during the coarsening stage ( $f_p = 0.4$ ,  $\rho_0 = 0.5$ ). Parameters:  $\mu = 1$ , translational diffusivity  $D_t = 0.4$ ,  $D_r = 2$ ,  $\sigma = 0.89$ , system size  $300 \times 300$ . Data courtesy of Gianmarco Spera.

#### 1. Bulk phase separation in scalar active matter

When considering systems whose large-scale behaviors are characterized by the conserved dynamics of a density field, possibly the simplest phase transition corresponds to condensation and the breaking of translational uniformity.

In many active particle contexts, condensation has been predicted theoretically (Fily and Marchetti, 2012; Mognetti *et al.*, 2013; Paliwal *et al.*, 2018; Redner *et al.*, 2013a,b; Spera *et al.*, 2023; Stenhammar *et al.*, 2014, 2015; Wysocki *et al.*, 2014), and observed experimentally (Buttinoni *et al.*, 2013; van der Linden *et al.*, 2019; Liu *et al.*, 2019; Palacci *et al.*, 2013; Theurkauff *et al.*, 2012), arising from the interplay between attractive, repulsive, and propulsion forces. When self-propulsion is weak, attractive forces between the particles can easily overcome activity, and the expected equilibrium phase transitions typically survives. This is illustrated in Fig. 2 using numerical simulations of self-propelled ABPs in the presence of a translational noise and Lennard-Jones (LJ) interactions. At  $f_p = 0$ , the system undergoes equilibrium liquid-gas phase separation. As  $f_p$  increases, the phase-separated region shrinks until activity overcomes the attractive forces, and the system turns into a homogeneous fluid. Surprisingly, at even larger propulsion forces, a reentrant phase transition into a phase-separated region is observed (Redner *et al.*, 2013a; Spera *et al.*, 2023).

The mechanism underlying this reentrant phase transition is MIPS, which is distinct from equilibrium phase separation and does not require attraction between the particles. Instead, MIPS results from the interplay between the tendency of active particles to accumulate

where they move slower and their slowdown at high density due to collisions and repulsive forces (Cates and Tailleur, 2015).

MIPS has been reported in a wealth of active systems and can arise from a variety of interactions: pairwise forces (Fily and Marchetti, 2012; Redner *et al.*, 2013b; Stenhammar *et al.*, 2014; Wysocki *et al.*, 2014), QS (Bäuerle *et al.*, 2018; Cates and Tailleur, 2013; Curatolo *et al.*, 2020; Liu *et al.*, 2011; Tailleur and Cates, 2008), chemotaxis (O’Byrne and Tailleur, 2020; Zhang *et al.*, 2021; Zhao *et al.*, 2023), or steric hindrance (Adachi and Kawaguchi, 2020; Agranov *et al.*, 2021; Dittrich *et al.*, 2021; Kourbane-Houssene *et al.*, 2018; Maggi *et al.*, 2021; Thompson *et al.*, 2011; Whitelam *et al.*, 2018). It has been extensively reviewed (Cates and Tailleur, 2015; Fodor and Marchetti, 2018; O’Byrne *et al.*, 2023; Stenhammar, 2021) and we focus here on its simplest hydrodynamic description.

## 2. A minimal hydrodynamic description of MIPS

MIPS was first observed in collections of RTPs interacting via quorum-sensing (QSAPs; see Fig. 3(a)) whose self-propulsion speed  $v_p = \mu f_p$  decreases rapidly enough as the local density increases (Tailleur and Cates, 2008). For this system, it is possible to derive a fluctuating hydrodynamics for the density field as

$$\partial_t \hat{\rho} = \nabla \cdot [\hat{\rho} \mathcal{D}_{\text{eff}} \nabla \mathbf{u} + \sqrt{2\hat{\rho} \mathcal{D}_{\text{eff}}} \mathbf{\Lambda}]. \quad (4)$$

In Eq. (4), the density field is constructed from the  $N$  particle positions as

$$\hat{\rho}(\mathbf{r}, t) \equiv \sum_{i=1}^N \delta[\mathbf{r} - \mathbf{r}_i(t)], \quad (5)$$

$\mathcal{D}_{\text{eff}}(\mathbf{r}, [\hat{\rho}]) = v^2(\mathbf{r}, [\hat{\rho}])\tau/d$  is the large-scale diffusivity,  $\mathbf{u}(\mathbf{r}, [\hat{\rho}]) = \log[\hat{\rho}(\mathbf{r})v(\mathbf{r}, [\hat{\rho}])]$  is a non-equilibrium chemical potential, and  $\mathbf{\Lambda}$  is a centered Gaussian white noise of unit variance and delta-correlated in space. The derivation of Eq. (4) relies on a diffusive approximation of the microscopic run-and-tumble dynamics (Cates and Tailleur, 2013; Solon *et al.*, 2015a; Tailleur and Cates, 2008) and on stochastic calculus (Dean, 1996; Solon *et al.*, 2015a).

In a system with a homogeneous density  $\rho_0$ , the chemical potential can be written as  $\mathbf{u} = \log[\rho_0 v(\mathbf{r}, [\rho_0])] \equiv f'(\rho_0)$ , where  $f(\rho_0)$  is a Landau-like free energy density. For all density values such that  $f''(\rho_0) < 0$ , a homogeneous system is linearly unstable and separates into liquid and gas phases. This instability defines a spinodal region. To predict the coexisting ‘binodal’ densities and the phase diagram of the system, one needs to consider inhomogeneous density profiles. The mapping onto an equilibrium theory then breaks down because  $\mathbf{u}$ , in general, cannot be written as the functional derivative of a

free energy  $\mathcal{F}[\rho]$ . To leading order in a gradient expansion, however, a predictive theory can be formulated to determine the phase diagram (Solon *et al.*, 2018a,b).

Active particles interacting via pairwise forces (PFAPs) provide another system for which an explicit coarse-graining of the microscopic dynamics is possible. In the presence of repulsive interactions, it has led to a predictive theory for MIPS. This case is significantly more involved than QSAPs but a series of articles have led to the understanding of the spinodal instability, first, and more recently to the prediction of the binodals (Fily and Marchetti, 2012; Redner *et al.*, 2013b; Solon *et al.*, 2018a,b, 2015c; Speck, 2021; Stenhammar *et al.*, 2014; Takatori and Brady, 2015).

An alternative route to account for MIPS is to follow phenomenological approaches and construct a hydrodynamic description for a fluctuating coarse-grained density field  $\rho$  that includes all terms allowed by symmetry (Witkowski *et al.*, 2014). At the fourth order in a gradient expansion, one obtains active model B+ dynamics (Tjhung *et al.*, 2018):

$$\partial_t \rho = -\nabla \cdot [\mathbf{J} + \sqrt{2DM} \mathbf{\Lambda}], \quad (6)$$

$$\mathbf{J}/M = -\nabla \left[ \frac{\delta \mathcal{F}}{\delta \rho} + \lambda |\nabla \rho|^2 \right] + \zeta (\nabla^2 \rho) \nabla \rho, \quad (7)$$

where  $\mathcal{F} = \int d^d \mathbf{r} [f(\rho) + \kappa |\nabla \rho|^2]$  and  $f(\rho)$  plays again the role of a Landau free energy density. All coefficients  $D$ ,  $M$ ,  $\kappa$ ,  $\lambda$  and  $\zeta$  depend in principle on  $\rho$ . The  $\lambda$  and  $\zeta$  terms both break time reversal symmetry (Nardini *et al.*, 2017; Tjhung *et al.*, 2018) and the dynamics in Eqs. (6)-(7) cannot be derived from a free energy as in regular model B. Active model B+ is thus a generalization of Eq. (4), which accounts for MIPS in a broader set of systems. Using the methods developed in (Solon *et al.*, 2018a,b), it is again possible to predict the coexisting densities of a fully phase-separated system. An interesting difference with equilibrium physics is that the interfacial terms contribute to the results (Witkowski *et al.*, 2014).

## 3. Beyond the simple MIPS scenario

Interestingly, Eqs. (6)-(7) predict a richer physics than the simple MIPS scenario discussed above: for large values of  $|\zeta|$ , one observes a reversed Ostwald ripening whereby small droplets grow at the expense of larger ones (Tjhung *et al.*, 2018). In the phase coexistence regime, this leads to a dense phase that contains droplets of the dilute phase evolving with complex dynamics. This is reminiscent of what has been observed in simulations of PFAPs, where the droplet sizes are found to be algebraically distributed, leading to a critical dense phase (Caporusso *et al.*, 2020; Shi *et al.*, 2020) shown Fig. 3(c).

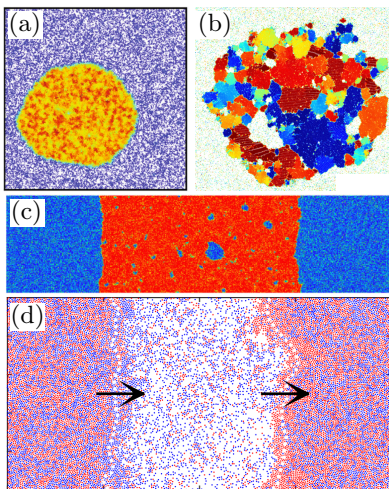


FIG. 3 (a) MIPS in ABPs interacting via quorum sensing showing a liquid-gas phase separation. Reproduced with kind permission of The European Physical Journal (EPJ) from (Solon *et al.*, 2015a). (b) MIPS in ABPs interacting via a stiff repulsion showing a mosaic of hexatic domains and gas inclusions in the dense phase. The color indicates the direction of the hexatic order. Reproduced with permission from (Caporusso *et al.*, 2020). (c) MIPS in ABPs interacting via harmonic repulsion showing a distribution of gas bubbles in the dense phase. Warmer colors indicate a higher density. Reproduced with permission from (Shi *et al.*, 2020). (d) MIPS in a mixture of ABPs and passive Brownian particles showing propagating interfaces in the direction indicated by the black arrows. Reproduced with permission from (Wysocki *et al.*, 2016).

Besides the nature of the phase-separated state, the critical properties of MIPS have also attracted attention. Conflicting results have been reported regarding the critical point (Speck, 2022). It has been measured and argued to have exponents either in the Ising universality class (Maggi *et al.*, 2022, 2021; Partridge and Lee, 2019) or another one (Caballero *et al.*, 2018; Siebert *et al.*, 2018), and the effect, or absence thereof, of bubbles on the critical point remains unclear (Caballero *et al.*, 2018).

The microscopic systems described above also display interesting properties beyond those captured solely by the dynamics of their density field, and thus fall outside the scope of this colloquium. For instance, the dense phases observed in ( $d = 2$ ) simulations of PFAPs have revealed a rich structure: they are found either in a disordered liquid form (Fily and Marchetti, 2012) for soft repulsive potentials, or as a mosaic of hexatic domains with different orientations for stiffer ones (see (Digregorio *et al.*, 2018; Redner *et al.*, 2013b) and Fig. 3(b)). Furthermore, the hexatic phase observed in the passive limit of this system survives the addition of activity (Digregorio *et al.*, 2018) and has attracted a lot of attention recently (Digregorio *et al.*, 2019). At high density, active systems also exhibit a glassy dynamics, which has

been observed experimentally (Angelini *et al.*, 2011; Garcia *et al.*, 2015; Klongvessa *et al.*, 2019) and numerically (Berthier *et al.*, 2017, 2019; Klongvessa *et al.*, 2019; Levis and Berthier, 2015).

Finally, rich physical phenomena occur in mixtures of scalar active systems. For example, mixtures of active and passive particles interacting via pairwise repulsion can demix (Ilker and Joanny, 2020; Weber *et al.*, 2016) or jointly undergo MIPS (Stenhammar *et al.*, 2015), while mixed species of QSAPs can either segregate or co-localize (Curatolo *et al.*, 2020). Out of equilibrium, one expects generically that the interactions between two species are non-reciprocal. Even for PFAPs, which obey Newton’s third law of action and reaction microscopically, the large-scale description of a mixture of active and passive particles features non-reciprocal couplings (Wittkowski *et al.*, 2017). When strong enough, the non-reciprocity gives rise to propagating patterns, as shown using a phenomenological theory (Saha *et al.*, 2020; You *et al.*, 2020) and observed in mixtures of active and passive ABPs (Wysocki *et al.*, 2016) (see Fig. 3(d)), as well as for mixtures of QSAPs (Dinelli *et al.*, 2022).

All in all, most results on the collective behaviors of scalar active matter have been established in idealized systems, invariant by translation and endowed with periodic boundary conditions. In equilibrium, when the correlation length is finite, obstacles and boundaries alter the system only in their immediate vicinity, which legitimates this approach. As we shall see in Section VI, the situation is very different for active system, where boundaries may have a far-reaching influence on bulk behaviors. Before we discuss this case, we first review the anomalous mechanical forces exerted by active systems on boundaries and inclusions, which are at the root of this important difference between active and passive systems.

### III. MECHANICAL FORCES ON CONFINING BOUNDARIES

In recent years, it has become evident that active systems display many anomalous properties when they interact with boundaries. Arguably, the simplest demonstration of this is obtained by placing an asymmetric mobile partition in a cavity comprising a homogeneous gas of self-propelled ellipses. One then observes a spontaneous compression of one side of the system, in violation of the second law of thermodynamics (see Fig. 4). By now, it has become clear that such phenomena can be rationalized in terms of the anomalous mechanical properties of active fluids, which we review in this section.

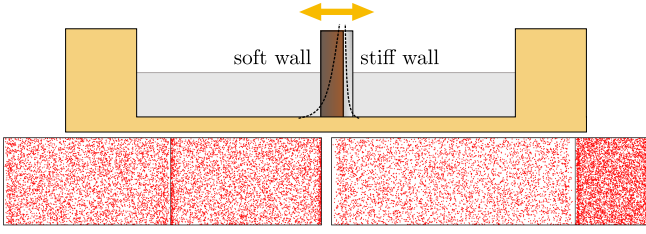


FIG. 4 **Top:** A mobile partition that is stiffer on one side divides the system into two compartments, each initially with equal density. Since the pressure depends on the wall's stiffness through Eq. (24), each side of the partition experiences a different force from the active particles. As a result, the mobile partition moves until the forces on both sides balance. This material was originally published in (Tailleur *et al.*, 2022) and has been reproduced by permission of Oxford University Press. For permission to reuse this material, please visit <http://global.oup.com/academic/rights>. **Bottom:** Numerical simulations corresponding to the setup described in the top panel using either circular ABPs (left panel) or elliptical ABPs (right panel). The absence of an equation of state (EOS) in the latter case is apparent from the spontaneous compression of one half of the system. Reproduced with permission from (Solon *et al.*, 2015b).

### A. Mechanical pressure on flat confining boundaries

Consider the simplest case of a two-dimensional gas of non-interacting active particles confined by a vertical flat wall localized at  $x = x_w$ , which we model by a repulsive potential  $V_w(x)$  that vanishes for  $x < x_w$  and diverges at larger values of  $x$ . The pressure exerted by the gas on the wall can be computed as:

$$P = \int_{x_b}^{\infty} dx \rho(x, y_b) \partial_x V_w(x), \quad (8)$$

where  $(x_b, y_b) \equiv \mathbf{r}_b$  corresponds to a point deep in the bulk of the active fluid,  $x_b \ll x_w$ , and  $\rho(\mathbf{r}, t) = \langle \sum_i \delta[\mathbf{r} - \mathbf{r}_i(t)] \rangle$  is the average number density (see Fig. 5). To determine  $P$ , it is natural to start from the dynamics of particle  $i$ , which reads

$$\dot{\mathbf{r}}_i = \mu \mathbf{f}_p^i - \mu \nabla V_w(\mathbf{r}_i) + \sqrt{2D_t} \boldsymbol{\eta}_i, \quad (9)$$

where  $\mathbf{f}_p^i \equiv f_p \mathbf{u}(\theta_i)$  is the particle propulsion force,  $\mu$  its mobility,  $D_t$  a translational diffusivity, and  $\boldsymbol{\eta}_i$  a centered Gaussian white noise of unit variance. The evolution of  $\rho$  then satisfies a conservation law

$$\partial_t \rho(\mathbf{r}, t) = -\nabla \cdot \mathbf{J}(\mathbf{r}, t), \quad (10)$$

where the current  $\mathbf{J}$  is given by

$$\mathbf{J} = \mu \mathbf{F}_a(\mathbf{r}) - \mu \rho(\mathbf{r}) \nabla V_w(\mathbf{r}) - D_t \nabla \rho(\mathbf{r}), \quad (11)$$

and  $\mathbf{F}_a \equiv \langle \sum_i \mathbf{f}_p^i \delta(\mathbf{r} - \mathbf{r}_i) \rangle$  is the active-force density. In the steady state, the confinement by a wall and the

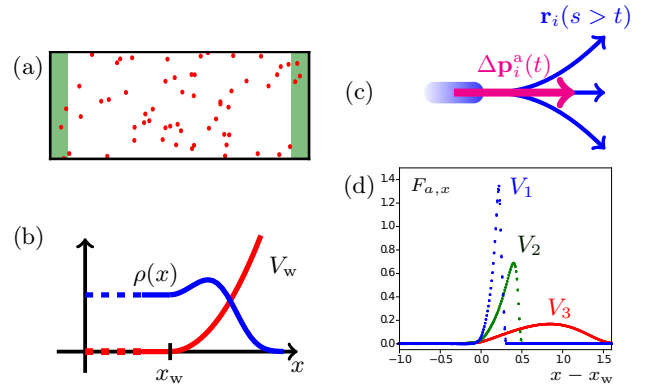


FIG. 5 (a) A simple setup to compute the pressure exerted by an active gas on confining walls consists of a  $2d$  box with periodic boundaries along  $y$  and a confining potential along  $x$ . (b) Schematic representation of the density of active particles and of the confining wall potential shown in panel (a). (c) Despite the fact that the active force is doing an isotropic random walk, it will transmit a non-zero average momentum to the active particle between any time  $s = t$  and  $s = +\infty$ . The corresponding ‘active’ impulse  $\Delta \mathbf{p}_i^a(t)$  is therefore nonzero. (d) The active force densities measured for three different confining potentials is non-zero close to a confining wall. The figure shows a clear dependence on the wall potential. In the presence of an EOS, the areas under the three curves are the same.

translational symmetry along the wall imply a vanishing current  $\mathbf{J} = 0$ . Using Eqs. (8) and (11), the pressure can then be written as

$$P = \frac{D_t}{\mu} \rho(\mathbf{r}_b) + \int_{x_b}^{\infty} dx \mathbf{F}_a(x, y_b). \quad (12)$$

The pressure exerted by the system on the wall is thus the sum of the passive ideal-gas pressure and a contribution stemming from the active force density, which is typically non-zero close to confining walls (See Fig. 5(d)).

Before considering the case of self-propelled ellipses shown in Fig. 4, we start with the simpler case of ABPs that undergo isotropic rotational diffusion everywhere in space,  $\dot{\theta}_i = \sqrt{2D_r} \eta_i^r$ , where  $\eta_i^r$  is a centered Gaussian white noise of unit variance. To make progress, it is useful to introduce the active impulse of particle  $i$ , which is the average momentum the particle will receive in the future from the substrate on which it is pushing. For a circular ABP, whose orientation is  $\mathbf{u}[\theta_i(t)]$  at time  $t$ , the active impulse can be computed as

$$\Delta \mathbf{p}_i^a \equiv \int_t^{\infty} ds f_p \overline{\mathbf{u}[\theta_i(s)]} = \frac{f_p}{D_r} \mathbf{u}[\theta_i(t)], \quad (13)$$

where the overline denotes an average over future histories, i.e., over  $\eta_i^r(s \geq t)$ , and we have used that  $\overline{\mathbf{u}[\theta_i(s)]} = \mathbf{u}[\theta_i(t)] \exp[-D_r(s-t)]$ . Even though the particle is undergoing a random walk, so that its average active force is zero, the active impulse at time  $t$  is non-zero because of persistence (see Fig. 5(c)). Direct algebra

then shows that the time evolution of the active impulse field  $\Delta\mathbf{p}^a(\mathbf{r}) \equiv \langle \sum_i \Delta\mathbf{p}_i^a \delta(\mathbf{r} - \mathbf{r}_i) \rangle$  is given by

$$\partial_t \Delta\mathbf{p}^a(\mathbf{r}) = -\mathbf{F}_a(\mathbf{r}) + \nabla \cdot \sigma_a(\mathbf{r}), \quad (14)$$

where

$$-\sigma_a \equiv \left\langle \sum_i \dot{\mathbf{r}}_i \otimes \Delta\mathbf{p}_i^a \delta(\mathbf{r} - \mathbf{r}_i) \right\rangle - D_t \nabla \otimes \Delta\mathbf{p}^a(\mathbf{r}) \quad (15)$$

is a tensor that measures the flux of active impulse. In the homogeneous isotropic bulk of the system, a direct computation shows that  $\sigma_a = \rho_b \mu f_p^2 / (2D_r) \mathbb{I}_d$ , where  $\mathbb{I}_d$  is the identity tensor. In the steady state, Eq. (14) shows that the density of active force is the divergence of the ‘active’ stress tensor  $\sigma_a$ :

$$\mathbf{F}_a(\mathbf{r}) = \nabla \cdot \sigma_a(\mathbf{r}). \quad (16)$$

Equation (16) has a simple interpretation: the active impulse acts as a ‘‘momentum reservoir’’ for the particle. To produce a non-zero density of active force in a region of space, incoming and outgoing fluxes of active impulse have to differ. Finally, the pressure takes the ideal gas law form

$$P = \rho(\mathbf{r}_b) \frac{D_t}{\mu} - \hat{\mathbf{x}} \cdot \sigma_a(\mathbf{r}_b) \cdot \hat{\mathbf{x}} = \rho_b T_{\text{eff}}, \quad (17)$$

where  $\rho_b \equiv \rho(\mathbf{r}_b)$ ,  $D_{\text{eff}} = D_t + (\mu f_p)^2 / 2D_r$  is the large-scale diffusivity of the particle,  $T_{\text{eff}} \equiv D_{\text{eff}} / \mu$  is an effective temperature<sup>2</sup>, and  $\hat{\mathbf{x}}$  is a unit vector in the  $x$  direction. The pressure can thus be written as the sum of a passive and an active stress, which is remarkable due to the absence of momentum conservation in the system. Since  $\partial_t \langle \mathbf{r}_i \otimes \mathbf{u}_i \rangle = \langle \dot{\mathbf{r}}_i \otimes \mathbf{u}_i \rangle - D_r \langle \mathbf{r}_i \otimes \mathbf{u}_i \rangle$ , one finds that, in a homogeneous bulk, the active stress tensor can be rewritten as

$$\sigma_a = - \left\langle \sum_i \mathbf{r}_i \otimes \mathbf{f}_p^i \delta(\mathbf{r} - \mathbf{r}_i) \right\rangle. \quad (18)$$

This expression was introduced in (Takatori *et al.*, 2014), where it was termed the ‘‘swim pressure’’. It can also be obtained using methods developed by Irving and Kirkwood (Yang *et al.*, 2014) or using a generalized virial theorem (Falasco *et al.*, 2016; Winkler *et al.*, 2015).

It is interesting to note that when the active force density satisfies Eq. (16), there is a relation in the steady state between the total current  $\mathbf{J}_{\text{tot}}$  flowing through the system and the total force  $\mathbf{F}_{\text{tot}}$  exerted by the particles on the boundary. To see this, integrate Eq. (11) over space to get that the total current  $\mathbf{J}_{\text{tot}} \equiv \int d^2\mathbf{r} \mathbf{r} \mathbf{J}(\mathbf{r})$  satisfies:

$$\mathbf{J}_{\text{tot}} = -\mu \int d^2\mathbf{r} \rho(\mathbf{r}) \nabla V_w(\mathbf{r}) \equiv -\mu \mathbf{F}_{\text{tot}}, \quad (19)$$

where we have used that  $\int d^2\mathbf{r} \mathbf{F}_a(\mathbf{r}) = 0$  due to Eq. (16). A more intuitive derivation of this result can be obtained by summing Eq. (9) over all particles and averaging over the steady-state distribution. One then gets

$$\mathbf{J}_{\text{tot}} = \left\langle \sum_i \dot{\mathbf{r}}_i \right\rangle = -\mu \left\langle \sum_i \nabla V_w(\mathbf{r}_i) \right\rangle = -\mu \mathbf{F}_{\text{tot}}, \quad (20)$$

where the sum of the active forces has vanished since the dynamics of the orientations are isotropic random walks decoupled from  $\mathbf{r}_i(t)$ —which, as will become clear below, is the reason why Eq. (16) holds. In flux-free systems, Eq. (20) thus implies that boundaries cannot exert any net total force on an active bath.

We note that Eq. (17) shows that the pressure is independent of the wall potential. This is remarkable since  $\mathbf{F}_a(\mathbf{r})$  depends on the choice of confining potential  $V_w(\mathbf{r})$  (see Fig. 5(d)). The underlying reason is that, since the dynamics of the particle orientation is independent from all other degrees of freedom, the total active impulse that the particle can transfer to the wall does not depend on the wall potential. The existence of an equation of state for the pressure can be generalized to ABPs interacting via pairwise forces and can be used to derive a mechanical theory for MIPS in such systems (Omar *et al.*, 2023; Solon *et al.*, 2018a,b, 2015c; Speck, 2021; Takatori *et al.*, 2014).

We note, however, that the derivation above does not account for the simulations reported in Fig. 4. One thus needs to go one step further and account for the ellipsoidal particle shapes by considering the torques  $\Gamma$  exerted by the walls on the particles:  $\dot{\theta}_i = \Gamma(\mathbf{r}_i, \theta_i) + \sqrt{2D_r} \eta_i^t$ . In this case, the time evolution of the active-force density  $\mathbf{F}_a(\mathbf{r})$  is given by:

$$\begin{aligned} \partial_t \mathbf{F}_a(\mathbf{r}) = & \left\langle \sum_i f_p \Gamma(\mathbf{r}_i, \theta_i) \mathbf{u}^\perp(\theta_i) \delta(\mathbf{r} - \mathbf{r}_i) \right\rangle - D_r \mathbf{F}_a(\mathbf{r}) \\ & - \nabla \cdot \left[ \left\langle \sum_i \dot{\mathbf{r}}_i \otimes \mathbf{f}_p^i \delta(\mathbf{r} - \mathbf{r}_i) \right\rangle \right], \end{aligned} \quad (21)$$

where  $\mathbf{u}^\perp(\theta) = \partial_\theta \mathbf{u}(\theta)$ . In the steady state, one finds

$$\mathbf{F}_a(\mathbf{r}) = \nabla \cdot \sigma_a^{\text{tf}} + \left\langle \sum_i \frac{f_p}{D_r} \Gamma(\mathbf{r}_i, \theta_i) \mathbf{u}^\perp(\theta_i) \delta(\mathbf{r} - \mathbf{r}_i) \right\rangle, \quad (22)$$

where  $\sigma_a^{\text{tf}} = - \left\langle \sum_i \dot{\mathbf{r}}_i \otimes \frac{\mathbf{f}_p^i}{D_r} \delta(\mathbf{r} - \mathbf{r}_i) \right\rangle$  is the flux of active impulse in the absence of torques. Equation (22) thus splits the contribution to the density of active forces between conserved and non-conserved parts, hence showing that wall-induced torques can be seen as sources or sinks of active impulse. Introducing  $\psi(\mathbf{r}, \theta) = \langle \sum_i \delta(\mathbf{r} - \mathbf{r}_i) \delta(\theta - \theta_i) \rangle$ , the pressure can be written as

$$P = \rho_b T_{\text{eff}} + \Delta P_w, \quad (23)$$

where  $\Delta P_w$  is a wall-dependent contribution given by

$$\Delta P_w = \frac{\mu f_p}{D_r} \int d\theta \int_{x_b}^{\infty} dx \psi(x, y_b, \theta) \Gamma(x, y_b, \theta) \sin \theta. \quad (24)$$

<sup>2</sup> We note, beyond the analogy with the ideal gas law,  $T_{\text{eff}}$  does not, in general, play any thermodynamic role in active systems.



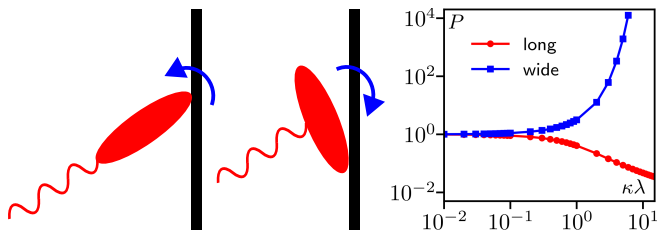


FIG. 6 **Left:** Schematic representation of an elliptic active particle hitting a wall. Depending on the aspect ratio, the collision rotates the particle in opposite directions, making it face parallel or toward the wall. **Right:** Mechanical pressure measured on the wall for non-interacting ABPs with an aspect-ratio parameter  $\kappa = |a^2 - b^2|/8$ , where  $a$  and  $b$  are the axis lengths of the ellipse. The wall is a confining harmonic potential of stiffness  $\lambda$ . Parameters:  $f_p = \mu = 1$ ,  $D_r = 0.5$ ,  $\lambda = 1$ , bulk density  $\rho = 1$ , system size  $20 \times 2$ . As suggested by the left panel, the pressure exerted by long particles ( $a > b$ ) is decreased by the wall torques, whereas that of wide particles ( $a < b$ ) is enhanced.

Importantly, the pressure is not independent of the wall anymore, which explains the spontaneous compression of the asymmetric piston shown in Fig. 4. Indeed, the piston is stalled when the pressures on both sides are equal, which requires  $\Delta P_{w_L}(\rho_L) = \Delta P_{w_R}(\rho_R)$ . When the left and right walls of the piston are different, this equality requires different densities on both sides of the piston.

The discussion above can be understood by thinking about the most commonly encountered active particles around us: pedestrians. Think about a small child running towards you. Stopping the child requires making its translational speed vanish, hence bringing the corresponding incoming momentum flux to zero. This corresponds to the drop of the passive momentum ( $\rho D_t/\mu$  in the case of an ideal gas). If the child keeps running while you are holding them, you have to absorb an additional momentum flux that the child is transferring from the ground onto you, which corresponds to the contribution of the active force in Eq. (12). Because many different strategies can be employed to stop the child from running, the active pressure will generically depend on the restraining adult, hence leading to the lack of an equation of state. This is how torques lead to a lack of equation of state, as illustrated in Fig. 6. For torque-free ABPs, because the dynamics of the active force is independent of all other degrees of freedom, the momentum flux they transfer to the wall through their active force before running away is always given by  $\mu f_p^2/2D_r$ , which leads to an equation of state. We note that this is an idealized limit and that, for dry active systems, the lack of equation of state is expected to be generic, a fact that has been confirmed experimentally (Junot *et al.*, 2017) for self-propelled discs (see Fig. 7). We stress that the lack of equation of state is not necessarily related to torques

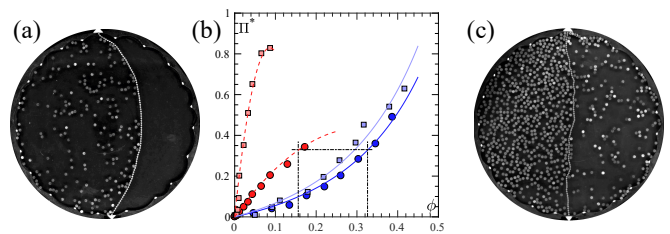


FIG. 7 **(a)** A flexible chain separates a system of vibrated grains into two cavities. The chain curvature is used to measure the pressure exerted by the particles confined in the left cavity, which can be either isotropic passive-like disks or anisotropic active disks. **(b)** Pressure  $\Pi$  measured as the packing fraction  $\phi$  is varied. For isotropic disks (blue),  $\Pi$  is in agreement with the equilibrium equation of states for hard disks (plain lines). For active disks (red), two types of chains made with links of different sizes measure different pressures (square and circle symbols), signaling the absence of an equation of state for the pressure. Dot-dashed line denotes positions where active and passive disks are in equilibrium at different densities, as shown in **(c)**. Reproduced with permission from (Junot *et al.*, 2017)

induced by confining walls: Aligning interactions and motility regulation have, for instance, also been shown to prevent the existence of an equation of state for the pressure (Solon *et al.*, 2015b).

## B. Curved and flexible boundaries

The anomalous mechanical properties of dry active systems are not restricted to the lack of an equation of state for flat walls. Indeed, even in cases where an equation of state exists, the local pressure exerted by active fluids on confining walls generically depend on the boundary shape (Fily *et al.*, 2014, 2015; Mallory *et al.*, 2014b; Nikola *et al.*, 2016; Yan and Brady, 2015). This can be traced back to the fact that, after colliding with a wall, active particles glide along it and accumulate in regions with higher curvatures (Fily *et al.*, 2014; Mallory *et al.*, 2014b). This leads to non-trivial density modulations and currents near the wall (Fily *et al.*, 2014, 2015; Mallory *et al.*, 2014b; Yan and Brady, 2015) that are illustrated in Fig. 8 using numerical simulations of ABPs interacting with a periodic soft-wall potential that vanishes for  $x < x_w$  and is otherwise given by

$$V(\mathbf{r}) = \frac{k}{2}[x - x_w(y)]^2 \text{ with } x_w(y) = x_0 + A \sin(2\pi y/L_p) \quad (25)$$

and  $L_p$  the period. Importantly, Fig. 8(d) shows that the pressure, measured as the force normal to the wall, depends on the exact location along the wall.

The difference between the point of highest pressure and lowest pressure,  $\delta P$ , is found numerically to be proportional to the curvature  $1/R$  at the tips of the sinusoidal wall, see Fig. 9. This is consistent with measure-

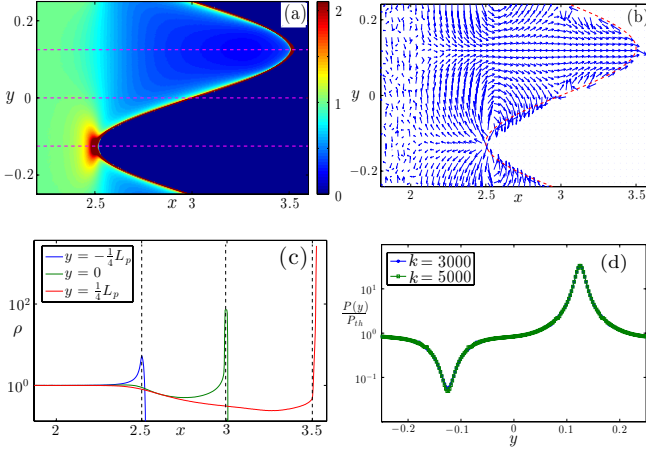


FIG. 8 Density (a) and current (b) of non-interacting ABPs near the right edge of the system with the curved-wall potential given in Eq. (25). Parameters:  $f_p = D_r = 24$ ,  $D_t = 0$ ,  $L_p = 0.5$ ,  $A = 0.5$ ,  $k = 10^3$ ,  $x_w = 3$ , and  $\mu = 1$ . The red dashed curve corresponds to  $x_w(y)$ . (c) Three cross sections of the particle density taken at the three horizontal dashed lines in (a). The vertical lines correspond to  $x_w(y)$ . (d) Pressure normal to the wall, normalized by Eq. (17), as a function of  $y$ , in the hard wall limit. Reproduced with permission from (Nikola *et al.*, 2016).

ments of the pressure exerted by an active ideal gas on a 2d circular cavity of radius  $R$  (Mallory *et al.*, 2014a; Sandford *et al.*, 2017; Yan and Brady, 2015). Moreover, recently, the corresponding finite-size correction was computed analytically and shown to be given by (Zakine *et al.*, 2020):

$$P(R) = P_b - \frac{\gamma}{R} + \mathcal{O}(R^{-1}), \quad (26)$$

where  $P_b = \rho_b T_{\text{eff}}$  is the pressure in an infinite system at density  $\rho_b$  and  $\gamma$  is the fluid-solid surface tension that can be computed as

$$\gamma \equiv \int_0^R dr \frac{\mu}{2} f_p^2 \tau \rho_b - \int_0^\infty dr \frac{\mu}{2} f_p^2 \tau \rho(r). \quad (27)$$

This result, which generalizes Laplace's law to active fluids, directly suggests that  $\delta P \simeq 2\gamma/R$ . On dimensional grounds, one can estimate the surface tension as  $\gamma \simeq -P_b \ell_p$ , with  $\ell_p$  the persistence length. This agrees semi-quantitatively with the measurements shown in Fig. 9. As shown by Eq. (27), the negative sign of  $\gamma$  is due to the tendency of active particles to accumulate at the wall. It is consistent with the overall sign of  $\delta P$ , which can also be understood heuristically as the active particles accumulate at concave regions of the wall. Note that the sign of  $\delta P$  shows that active particles tend to exert forces on curved boundaries that would amplify the deformation of a flexible boundary, as discussed below.

Interestingly, for walls that are not reflection-symmetric, a net shearing force develops parallel to the

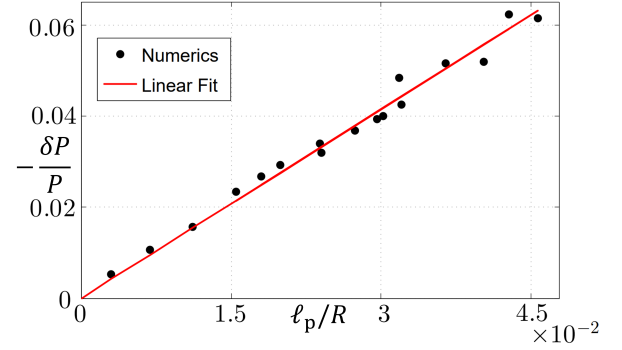


FIG. 9 Difference  $\delta P$  between the pressure at the concave and convex apices of the curved-wall potential given in Eq. (25), as the radius of curvature  $R = L_p/(4\pi^2 A)$  is varied. The red line is a linear fit of the data leading to a slope  $\sim 1.3$ . Numerical data were obtained using simulations of ABPs with  $f_p = 0.75$  and  $\mu = D_r = 1$ . Wall parameters in the ranges  $A \in [3.1 \cdot 10^{-3}, 3.3 \cdot 10^{-2}]$  and  $L_p \in [3.6, 5.5]$  were used, with  $k = 2 \cdot 10^4$ . Dimensional analysis predicts a slope of 2. Reproduced with permission from (Nikola *et al.*, 2016).

wall (Nikola *et al.*, 2016). It can be understood as a consequence of a ratchet effect (Ai and Wu, 2014; Angelani *et al.*, 2011; Reichhardt and Reichhardt, 2013): The breaking of time-reversal symmetry by the active particles coupled to a breaking of an inversion symmetry leads to a steady-state current along the wall. In turn, Eq. (11) tells us that such a current will generically be associated with a force tangential to the wall. This explains the spontaneous rotation of microscopic gears observed in simulations (Angelani *et al.*, 2009) and experiments (Di Leonardo *et al.*, 2010; Sokolov *et al.*, 2010).

The dependence of the active pressure on the boundary shape is exemplified by considering the behavior of flexible elastic objects inside an active fluid. For concreteness, first consider a flexible partition whose ends are held at walls at the top and bottom of a container filled with active particles. Once a fluctuation creates a local deformation in the filament, a finite pressure difference  $\Delta P$  develops between its two sides due to the difference in active forces exerted on the two sides of the apex. This tends to increase the deformation and is opposed by the elasticity of the flexible partition. The outcome of this competition can be understood by considering the linearized dynamics of the partition, characterized by a Monge representation  $h(x, t)$ . Because the accumulation of active particles is proportional to the curvature of a confining interface (Fily *et al.*, 2014; Nikola *et al.*, 2016), one expects  $\Delta P \propto \nabla^2 h$ , leading to (Nikola *et al.*, 2016):

$$\partial_t h(x, t) = (T - \kappa) \nabla^2 h(x, t) - \kappa_b \nabla^4 h(x, t), \quad (28)$$

where  $T$  and  $\kappa_b$  are the line tension and bending rigidity, respectively, and  $\kappa$  is a coefficient that measures the particle activity. Equation (28) shows that for large activity, when  $\gamma > T$ , a horizontal filament is unstable to fluctuations above a characteristic length  $\lambda \propto \sqrt{\kappa_b/(\kappa - T)}$ .

For short filaments, one thus expects that the rigidity keeps the filament straight, whereas long filaments are expected to be unstable. This has indeed been observed both in simulations and experiments (Junot *et al.*, 2017; Nikola *et al.*, 2016), where the instability has been shown to coarsen and lead to a deformation of the filament with a wavelength set by the system size. For an unpinned passive flexible filament in an active medium, an even richer scenario has been reported in both simulations and experiments (Anderson *et al.*, 2022; Nikola *et al.*, 2016). As the length of the filament increases, the instability discussed above first leads to a left-right asymmetry and the spontaneous formation of a parachute-like structure (Harder *et al.*, 2014; Shin *et al.*, 2015); somewhat reminiscent of a sail blowing in the wind, except with the wind itself generated by the curving filament. The pressure difference on the two sides of the filament then generates a net propelling force and turns the filament into an emergent active particle. Upon a further increase in length, a full period of the unstable mode develops, leading to short-lived spontaneous rotors. Finally, very long filaments are found to lead to folded structures.

#### IV. OBSTACLES AND LOCALIZED INCLUSIONS

An even richer physics has been reported when considering the mechanical interplay between active particles and obstacles *immersed* in active fluids. Arguably, the first observation for this was the experimental study of *asymmetric obstacles* by Galajda and co-workers (Galajda *et al.*, 2007), which demonstrated that an array of V-shaped obstacles placed in a bacterial bath leads to the accumulation of bacteria on one side of the array (see Fig. 10). In this section, we discuss how a mechanical perspective accounts for the induced organization of the bacterial fluid and how to account for more general situations. In particular, we focus on the universal aspects of the large-scale density modulation and current induced by obstacles and not on the rich physics that can be observed in the near field, at distances  $\mathcal{O}(\ell_p)$  from the obstacle, which has attracted a lot of attention (Kaiser *et al.*, 2012; Ni *et al.*, 2015; Potiguar *et al.*, 2014; Speck and Jayaram, 2021; Wysocki and Rieger, 2020; Yan and Brady, 2018; Zaeifi Yamchi and Naji, 2017) and has already been reviewed (Bechinger *et al.*, 2016).

We start with the case of a single obstacle immersed in an infinite active fluid and show how a multipole expansion allows one to predict the far-field structure of density and current fields. A simple picture emerges in which the local asymmetry of the obstacle induces a ratchet current that mass-conservation turns into long-range density and current modulations. Mathematically, the relation between the force monopole exerted by the obstacle on the active fluid and the induced current flow is identical to that between electrostatic dipoles and fields. Next, we

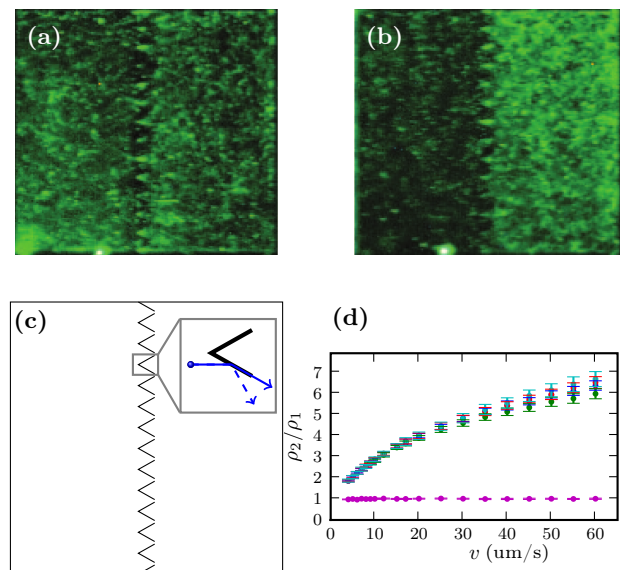


FIG. 10 (a)-(c) A uniform density of bacteria at the beginning of the experiment (a) becomes inhomogeneous at late times (b) in a 2d microfluidic chamber split into two compartments by an array of asymmetric obstacles, schematically depicted in (c). (d) Ratio between the densities of bacteria in the right ( $\rho_2$ ) and left ( $\rho_1$ ) sides of the cavity shown in (c), measured using numerical simulations of RTPs whose self-propulsion speed  $v$  is varied. All dimensions match the experiment: the enclosures dimensions are  $L \times H = 400\mu\text{m} \times 400\mu\text{m}$ , the arms of the funnels are  $27\mu\text{m}$  long and their apex angle is  $\pi/3$ , the funnels are separated by gaps  $3.8\mu\text{m}$  wide. The tumbling rate of the RTPs is set to  $\alpha = 1\text{s}^{-1}$ . The overlapping red, blue, green, and cyan symbols are obtained by varying  $H$  and the left and right chambers width,  $L_L$  and  $L_R$ , respectively, with  $(L_R, L_L, H) \in \{(200, 200, 400), (400, 400, 400), (200, 200, 800), (400, 200, 400)\}$ . The vertical density of obstacles is kept constant. The rectification of bacterial density is thus independent of finite-size effects. In all simulations, RTPs align with the walls upon collision (solid line inside the inset of panel (c)). When the RTPs instead experience specular reflection upon collision, as shown by the dashed line inside the inset of panel (c), a uniform density field is measured (magenta symbols). This is consistent with the fact that collisions are the sole irreversible process in these simulations. (a-b) were reproduced with permission from (Galajda *et al.*, 2007). (c-d) were reproduced with permission from (Tailleur and Cates, 2009).

turn to consider the effect of boundary conditions and show how an image theorem allows generalizing the results to simple cases like periodic or closed boundary conditions. Then, we discuss how the above leads to long-range non-reciprocal interactions between inclusions in an active fluid. Finally, we discuss the case of mobile inclusions and review recent works on passive tracers and possible dynamics arising from interactions mediated by active baths.

### A. A single obstacle in an infinite system

We consider  $N$  non-interacting ABPs in the presence of an obstacle modelled by an external potential  $V(\mathbf{r})$ , localized on a compact support near  $\mathbf{r} = 0$ . In  $d$  space dimensions, the average number density of particles at position  $\mathbf{r}$  with an orientation  $\mathbf{u}$ ,  $\mathcal{P}(\mathbf{r}, \mathbf{u})$ , evolves according to:

$$\partial_t \mathcal{P}(\mathbf{r}, \mathbf{u}) = -\nabla \cdot [\mu f_p \mathbf{u} \mathcal{P} - \mu \mathcal{P} \nabla V - D_t \nabla \mathcal{P}] + D_r \Delta_{\mathbf{u}} \mathcal{P}, \quad (29)$$

where  $\Delta_{\mathbf{u}}$  is the spherical Laplacian. Integrating over the orientation  $\mathbf{u}$  leads to Eqs. (10) and (11) with  $V_w$  replaced by  $V$ . Far away from the obstacle, i.e. when  $|\mathbf{r}| \gg \ell_p$ , the active dynamics is diffusive at large scales so that  $\mathbf{J} \simeq \mathbf{J}_D \equiv -D_{\text{eff}} \nabla \rho$ , where  $D_{\text{eff}} = D_t + (\mu f_p)^2 / d D_r$  (Cates and Tailleur, 2013). We then introduce

$$\delta \mathbf{J} \equiv \mathbf{J} - \mathbf{J}_D = \mu \mathbf{F}_a - \mu \rho \nabla V + (D_{\text{eff}} - D_t) \nabla \rho, \quad (30)$$

which measures the difference between  $\mathbf{J}$  and its diffusive approximation. Intuitively, we expect  $\delta \mathbf{J}$  to vanish in the bulk and to be significant in the vicinity of the obstacle, for  $|\mathbf{r}| \lesssim \ell_p$ . We can then rewrite the conservation equation in the steady state,  $\nabla \cdot \mathbf{J} = 0$ , as

$$D_{\text{eff}} \nabla^2 \rho = \nabla \cdot \delta \mathbf{J}(\mathbf{r}). \quad (31)$$

Equation (31) is a Poisson equation for the density field with a source term  $\nabla \cdot \delta \mathbf{J}(\mathbf{r})$  localized around the obstacle. Its solution is

$$\rho(\mathbf{r}) = \rho_b + \frac{1}{D_{\text{eff}}} \int d^d \mathbf{r}' G(\mathbf{r}, \mathbf{r}') \nabla \cdot \delta \mathbf{J}(\mathbf{r}'), \quad (32)$$

where  $G(\mathbf{r}, \mathbf{r}')$  is the Green's function of the Laplacian in  $d$  space dimensions. To proceed, we employ a multipole expansion of Eq. (32) to determine the leading contribution in the far-field limit,  $|\mathbf{r}| \gg \ell_p$ , using all the terms entering  $\nabla \cdot \delta \mathbf{J}$ . Using Eq. (16) and (30), one sees that the leading order contribution is given by  $\delta \mathbf{J}(\mathbf{r}) \simeq -\mu \rho(\mathbf{r}) \nabla V(\mathbf{r})$ . Introducing the force monopole

$$\mathbf{p} = - \int d^d \mathbf{r}' \rho(\mathbf{r}') \nabla V(\mathbf{r}'), \quad (33)$$

and carrying out explicitly the multipole expansion of Eq. (32), one then finds that the leading-order far-field density and current are given by

$$\rho(\mathbf{r}) = \rho_b + \frac{\beta_{\text{eff}} \mathbf{r} \cdot \mathbf{p}}{S_d r^d} + \mathcal{O}(r^{-d}), \quad (34)$$

$$\mathbf{J}(\mathbf{r}) = \frac{\mu}{S_d} \frac{d(\hat{\mathbf{r}} \cdot \mathbf{p}) \hat{\mathbf{r}} - \mathbf{p}}{r^d} + \mathcal{O}(r^{-(d+1)}), \quad (35)$$

where  $\beta_{\text{eff}} \equiv 1/T_{\text{eff}} = \mu/D_{\text{eff}}$  and  $S_d = (2\pi^{d/2})/\Gamma(d/2)$ . As usual in multipole expansions, Eq. (34) is the solution of

$$D_{\text{eff}} \nabla^2 \rho = \nabla \cdot [\mu \mathbf{p} \delta(\mathbf{r})]. \quad (36)$$

We note that Eq. (34) predicts a universal density modulation and current induced by an obstacle that exerts a non-vanishing force monopole  $\mathbf{p}$  on the active fluid. The determination of  $\mathbf{p}$ , on the other hand, depends on the details of the problem and requires an explicit derivation of the microscopic structure of  $\rho(\mathbf{r})$  in the vicinity of the obstacle. This is, in general, a very hard problem with very few exact results (de Pirey and van Wijland, 2023). We also note that if  $\mathbf{p} = 0$ , higher orders in the multipole expansion have to be considered (Baek *et al.*, 2018). When the obstacle is spherical, the density modulation and current vanish at all orders in the multipole expansion.

The above derivation shows how forces exerted by obstacles lead to large-scale ratchet currents. Since the pressure admits an equation of state—because the active force density can be written as the divergence of a local stress tensor—there is an exact relation between forces and current generated by obstacles. Integrating Eq. (11) over the full space indeed shows that

$$\mathbf{J}_{\text{tot}} \equiv \int d^d \mathbf{r} \mathbf{J}(\mathbf{r}) = \mu \mathbf{p}, \quad (37)$$

where we have used that  $\mathbf{F}_a(\mathbf{r}) = \nabla \cdot \sigma_a$  and the divergence theorem to show that the contribution of the active force vanishes when integrated over the full space. This result is the direct counterpart to Eq. (20) for the case of an isolated obstacle.

While the above formulation pertained to noninteracting ABPs. The result generalizes to homogeneous active fluids with pairwise interparticle forces (Granek *et al.*, 2020).

### B. Finite systems and boundary conditions

So far, we have considered the case of an isolated object in an infinite system and shown that asymmetric obstacles induce long-range density modulations and currents. In turn, this implies that some care has to be taken when finite systems of linear size  $L$  are considered, even when  $L \gg \ell_p$ . We now discuss several such scenarios that have been explored in the literature.

For periodic boundary conditions, when  $L \gg \ell_p$ , one can show that the system is equivalent to an infinite periodic lattice of obstacles (Granek *et al.*, 2020). Interestingly, the density and current fields, as well as the value of the force monopole  $\mathbf{p}$ , differ between infinite and periodic systems by corrections of order  $\mathcal{O}(L^{-(d+2)})$  (Speck and Jayaram, 2021). For  $L \lesssim \ell_p$ , the far-field expansion is naturally invalid. Numerical simulations and a scaling argument reveal that, for  $d = 2$ , the force monopole  $\mathbf{p}$  grows as  $\sim L^2$  until it saturates at an asymptotic value for  $L \gg \ell_p$  (Speck and Jayaram, 2021).

Another scenario that was considered is the effect of confining flat hard walls. The derivation of Sec. IV.A can

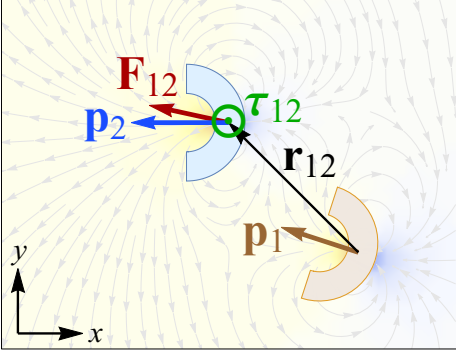


FIG. 11 Schematic diagram of two interacting asymmetric passive obstacles. Obstacle  $O^{(1)}$  (orange) is placed at  $\mathbf{X}_1$  and obstacle  $O^{(2)}$  (blue) is placed at  $\mathbf{X}_2$  (black) and we denote by  $\mathbf{r}_{12}$  their separation. Superimposed currents are shown in gray streamlines, and density modulations are shown with a blue-to-red colormap. Reproduced with permission from (Granek *et al.*, 2020)

be extended to this case—despite non-trivial boundary conditions—and, for a single obstacle displaced by  $\mathbf{X} = X\hat{\mathbf{x}}$  from a hard wall at  $x = 0$ , Eq. (32) still holds in the far field of both the obstacle and the wall (Ben Dor *et al.*, 2022a). The Green’s function  $G$  is, however, replaced by that of the Laplacian in a half-plane. To leading order in the limit  $|\mathbf{r} - \mathbf{X}| \gg \ell_p$  and  $X \gg \ell_p$ , the solution is given by:

$$\rho(\mathbf{r}) = \rho_b + \frac{\beta_{\text{eff}}}{S_d} \left[ \frac{(\mathbf{r} - \mathbf{X}) \cdot \mathbf{p}}{|\mathbf{r} - \mathbf{X}|^d} + \frac{(\mathbf{r} - \mathbf{X}^*) \cdot \mathbf{p}^*}{|\mathbf{r} - \mathbf{X}^*|^d} \right] + \mathcal{O}\left(|\mathbf{r} - \mathbf{X}|^{-d}, X^{-d}\right). \quad (38)$$

where  $\mathbf{p}^*$  and  $\mathbf{X}^*$  are the images of  $\mathbf{p}$  and  $\mathbf{X}$  with respect to the wall, respectively. Note that Eq. (38) holds with the force monopole  $\mathbf{p}$  given by its infinite-system value. Indeed, the corrections to  $\mathbf{p}$  due to the image obstacle enter at order  $\mathcal{O}(X^{-(d-1)})$ . Eq. (38) was also shown to hold when the obstacle is on the wall, so that  $\mathbf{X} = 0$ , with  $\mathbf{p}$  parallel to the wall (Ben Dor *et al.*, 2022b). Finally, the derivation was also carried out for a circular cavity, as will be discussed in Sec. IV.E.

### C. Non-reciprocal mediated interactions.

Since isolated obstacles create long-range density modulations, it is natural to expect that several obstacles immersed in the same active fluid will experience long-range mediated interactions. These turn out to be *non-reciprocal* and can be derived as follows. Consider two obstacles,  $O^{(1)}$  and  $O^{(2)}$ , fixed at positions  $\mathbf{X}^{(1)}$  and  $\mathbf{X}^{(2)}$ , respectively, and denote by  $\mathbf{r}_{12}$  their separation (see Fig. 11). The effect of  $O^{(1)}$  on  $O^{(2)}$  can be quantified by an emergent interaction force  $\mathbf{F}_{12}$ , which can be identified as the net residual force exerted on  $O^{(2)}$  due to the

introduction of  $O^{(1)}$  into the bath:

$$\mathbf{F}_{12} \equiv \mathbf{p}_2^0 - \mathbf{p}_2, \quad (39)$$

where  $-\mathbf{p}_k \equiv \int d^d \mathbf{r} \rho(\mathbf{r}) \nabla V_k(\mathbf{r} - \mathbf{X}^{(k)})$  is the net force exerted by the active bath on  $O^{(k)}$ , and  $\mathbf{p}_2^0 = \mathbf{p}_2|_{V_1=0}$  is the force on  $O^{(2)}$  in the absence of  $O^{(1)}$ . Inspection of Eq. (33) shows that  $\mathbf{F}_{12}$  is directly connected to the density modulation induced by  $O^{(1)}$  in the vicinity of  $O^{(2)}$ . For large separations  $r_{12}$ , the leading order contribution of this modulation is a local shift of the average density:

$$\delta\rho_1(\mathbf{X}_2) = \frac{\beta_{\text{eff}}}{S_d} \frac{\mathbf{r}_{12} \cdot \mathbf{p}_1}{r_{12}^d} + \mathcal{O}(r_{12}^{-d}). \quad (40)$$

Due to the linearity of Eq. (32), the force monopole exerted by  $O^{(2)}$  is modified as

$$\mathbf{p}_2 = \frac{\rho_b + \delta\rho_1(\mathbf{X}_2)}{\rho_b} \mathbf{p}_2^0. \quad (41)$$

Inserting this into Eq. (39) results in

$$\mathbf{F}_{12} = -\frac{\beta_{\text{eff}}}{S_d} \frac{\mathbf{r}_{12} \cdot \mathbf{p}_1^0}{\rho_b r_{12}^d} \mathbf{p}_2^0 + \mathcal{O}(r_{12}^{-d}), \quad (42)$$

where we have used  $\mathbf{p}_k = \mathbf{p}_k^0 + \mathcal{O}(r_{12}^{-(d-1)})$  and  $\mathbf{p}_1^0 = \mathbf{p}_1|_{V_2=0}$ .  $\mathbf{F}_{21}$  can be obtained by exchanging the indices  $1 \leftrightarrow 2$  in Eq. (42). Importantly, the equation implies that  $\mathbf{F}_{21} \neq -\mathbf{F}_{12}$ , i.e. the bath-mediated interactions are *non-reciprocal*.

Note that the leading-order interactions require both obstacles to be asymmetric so that  $\mathbf{p}_k^0 \neq 0$ . Nonetheless, when  $O^{(2)}$  is symmetric, it still experiences a force from an asymmetric  $O^{(1)}$  because the latter induces a density gradient in the vicinity of  $O^{(2)}$  (Baek *et al.*, 2018). Finally, we note that, while two isotropic obstacles only experience short-range interactions, long-range interactions can also emerge even if all  $\mathbf{p}_k^0$  vanish. For example, rods generate density modulations at order  $r_{12}^{-d}$  (Baek *et al.*, 2018).

So far, we have considered dilute active fluids, but these derivations extend to the case of active bath particles subject to pairwise interactions (Granek *et al.*, 2020). Furthermore, a similar expansion has been derived for the interaction torque  $\mathbf{n}_{12}$  between the obstacles (Baek *et al.*, 2018). The results also extend to multiple obstacles, yielding additive interactions to leading order in the far field.

### D. Mobile obstacles and dynamics

So far, we have discussed the case in which obstacles are fixed in space. However, there is also considerable interest in the dynamics of mobile obstacles, referred to as passive tracers in active baths. While a body of works

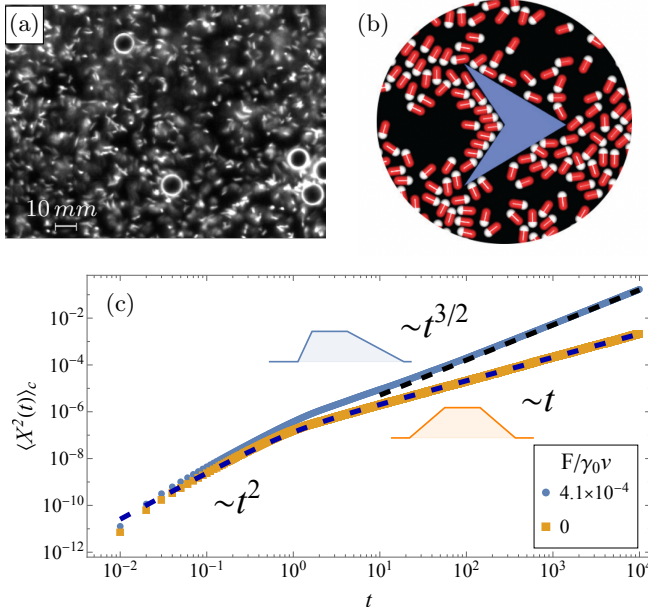


FIG. 12 (a) Passive polystyrene tracers immersed in a quasi-two-dimensional bacterial bath. Adapted with permission from (Wu and Libchaber, 2000). (b) Simulation snapshot of a V-shaped passive tracer in a two-dimensional active bath. Holding the tracer orientation fixed leads to an average directed motion to the right with velocity  $\propto -\mathbf{p}$ . Reproduced with permission from (Angelani and Di Leonardo, 2010). (c) Mean-square displacement for an adiabatic passive tracer in a one-dimensional active bath (microscopic simulations). Symmetric tracer (orange symbols): a transition from short-time ballistic motion to long-time diffusive is observed. Blue dashed line: the Wu-Libchaber model Eq. (45), with the exact calculation of the diffusivity  $D_T$  from the adiabatic theory (see text) and a fit leading to  $\tau = 0.41$ . Asymmetric tracer (blue symbols) shows a long-time superdiffusion. Black dashed line: the prediction Eq. (52) (no fitting parameters). All bath parameters are set to unity. Reproduced with permission from (Granek *et al.*, 2022).

focused on the effect of long-range hydrodynamic interactions in wet active baths (see, e.g. (Chen *et al.*, 2007; Kanazawa *et al.*, 2020; Kurihara *et al.*, 2017; Kurtuldu *et al.*, 2011; Leptos *et al.*, 2009; Thiffeault, 2015; Zaid *et al.*, 2011)), here, we focus on (dry) scalar active matter with, at most, short-range interactions.

To write down the emerging equations of motion of a tracer, we invoke an adiabatic limit where the motion of the tracer is so slow that the statistics of the forces exerted by the bath are indistinguishable from those exerted on a fixed tracer. In the overdamped limit, the dynamics of the tracer can then be described using a generalized Langevin equation (Feng and Hou, 2023; Granek *et al.*, 2022; Maes, 2020; Reichert *et al.*, 2021; Reichert and Voigtmann, 2021; Shea *et al.*, 2022):

$$\int_0^t dt' \gamma_{ij}(t-t') \dot{X}_j(t') = f_i(t), \quad (43)$$

where  $\gamma_{ij}(t)$  is a memory kernel,  $f_i(t)$  is a fluctuating force, and summation over  $j$  is implied. In Eq. (43), the left-hand-side is the friction force exerted by the bath, i.e. the average contribution to the force due to the motion of the tracer, while the right hand side contains both the net force exerted on a fixed tracer and the fluctuations of the force exerted by bath particles. Unlike in equilibrium,  $\langle \mathbf{f}(t) \rangle$  is generically non-zero for asymmetric tracers.

Within a systematic adiabatic expansion (D'Alessio *et al.*, 2016), the memory kernel  $\gamma_{ij}(t)$  is given by an Agarwal-Kubo-type formula

$$\gamma_{ij}(t) = \langle f_i(t) \partial_{X_j} \log P_s(\{\mathbf{r}_k(0) - \mathbf{X}, \mathbf{u}_k\}) |_{\mathbf{X}=0} \rangle_c^s, \quad (44)$$

where  $\mathbf{r}_k$  and  $\mathbf{u}_k$  are the positions and orientations of the bath particles,  $P_s(\{\mathbf{r}_k - \mathbf{X}, \mathbf{u}_k\})$  is their many-body steady-state distribution, and  $\langle \cdot \rangle^s$  denotes an average with respect to an ensemble in which the tracer is held fixed. The subscript  $c$  indicates a connected correlation function, i.e.,  $\langle AB \rangle_c = \langle AB \rangle - \langle A \rangle \langle B \rangle$ .

Likewise, the statistics of the fluctuating force  $\mathbf{f}(t)$  are given by those of  $\sum_k \nabla V(\mathbf{r}_k - \mathbf{X})$  computed with the tracer held fixed, and where  $V$  the interaction potential between the tracer and the active particles. For passive baths, the Boltzmann distribution  $P_s(\{\mathbf{r}_k - \mathbf{X}, \mathbf{u}_k\}) \propto e^{-\beta \sum_k V(\mathbf{r}_k - \mathbf{X})}$  recovers from Eq. (44) the fluctuation-dissipation relation  $\gamma_{ij}(t) = \beta \langle f_i(t) f_j(0) \rangle$ . Out of equilibrium, the relation is generically broken.

## 1. Phenomenological description of symmetric tracers

For isotropic tracers, it is common to use a heuristic suggestion by Wu and Libchaber to describe their experiments on passive tracers (see (Wu and Libchaber, 2000) and Fig. 12(a)). They postulated  $\gamma_{ij} = 2\Gamma_T \delta(t-t') \delta_{ij}$  and  $\langle f_i(t) f_j(0) \rangle_c = D_T \Gamma_T^2 e^{-t/\tau_1} / \tau_1 \delta_{ij}$ , with  $\tau_1$  a characteristic relaxation time and  $D_T$  a diffusion coefficient (Maggi *et al.*, 2017). Namely, the motion of the tracer behaves as an active particle with a mean-square displacement  $\langle \mathbf{X}^2(t) \rangle_c$  given by

$$\langle \mathbf{X}^2(t) \rangle_c = 2dD_T [t - \tau_1(1 - e^{-t/\tau_1})]. \quad (45)$$

This describes a crossover between a short-time ballistic motion ( $\sim t^2$ ) and a long-time diffusive motion ( $\sim t$ ), that is illustrated in Fig. 12(c). In the long-time limit, the particle diffuses as  $\langle \mathbf{X}^2(t) \rangle_c \sim 2dD_T t$ .

## 2. The Markovian approximation

The long-time behavior can be obtained through more systematic methods, starting from microscopic models and using Taylor's dispersion theory (Burkholder and Brady, 2017, 2019; Peng and Brady, 2022) or singular

perturbation methods (Jayaram and Speck, 2023; Solon and Horowitz, 2022). Assuming that  $\gamma_{ij}$  and  $\langle f_i(t)f_j(0) \rangle_c$  decay exponentially in time, this leads to a Markovian approximation of Eq. (43) of the form

$$0 = -\Gamma_{ij}\dot{X}_j(t) + \xi_i(t). \quad (46)$$

Here,  $\xi(t)$  is a Gaussian white noise that satisfies  $\langle \xi_i(t)\xi_j(0) \rangle_c = 2I_{ij}\delta(t)$  while the friction coefficient  $\Gamma_{ij}$  and noise intensity  $I_{ij}$  are given by the Green-Kubo relations

$$\Gamma_{ij} = \int_0^\infty dt \gamma_{ij}(t), \quad (47)$$

$$I_{ij} = \int_0^\infty dt \langle f_i(t)f_j(0) \rangle_c^s. \quad (48)$$

This recovers the long-time diffusive behavior postulated by Wu and Libchaber.

Within the Markovian approximation and in the isotropic case where  $I_{ij} = I\delta_{ij}$  and  $\Gamma_{ij} = \Gamma_T\delta_{ij}$ , one can identify an effective tracer temperature by  $T_T = I/\Gamma_T = D_T\Gamma_T$ . Interestingly, for hard-core tracers, the interpretation of  $T_T$  extends to an effective fluctuation-dissipation relation  $\gamma_{ij}(t) \simeq T_T^{-1}\langle f_i(t)f_j(0) \rangle_c$  despite the system being out of equilibrium at the microscopic scale (Solon and Horowitz, 2022). We note, however, that in contrast to equilibrium systems, the effective temperature depends on the properties of the tracer.

Note that, to model a tracer that is also in contact with a passive (Markovian) bath, one adds a thermostat  $-\Gamma_{\text{th}}\dot{X}_i(t) + \sqrt{2\Gamma_{\text{th}}T_{\text{th}}}\eta_i(t)$  to Eqs. (43) and (46). The effective temperature then modifies straightforwardly to (Granek *et al.*, 2022; Solon and Horowitz, 2022)

$$T_T = \frac{I + \Gamma_{\text{th}}T_{\text{th}}}{\Gamma_T + \Gamma_{\text{th}}} = \frac{\Gamma_T}{\Gamma_T + \Gamma_{\text{th}}}T_a + \frac{\Gamma_{\text{th}}}{\Gamma_T + \Gamma_{\text{th}}}T_{\text{th}}, \quad (49)$$

where  $T_a \equiv I/\Gamma_T$  is the active contribution.

The case of soft tracer brings in interesting differences, as was recently shown in  $d = 1$  (Granek *et al.*, 2022). First, the fluctuation-dissipation relation only survives in the limit of a shallow wide tracer, for which the system converges to an equilibrium distribution  $\rho(\mathbf{r}) \propto e^{-V(\mathbf{r})/T_{\text{eff}}}$  such that  $T_a = T_{\text{eff}} = D_{\text{eff}}/\mu$ . Then, for small tracers, the local structure of the active bath around the tracer may enhance its motion and lead to an effective *negative friction coefficient*  $\Gamma_T$  (Granek *et al.*, 2022). Microscopic simulations and a self-consistent calculation of the nonlinear tracer response reveal that the negative friction induces a spontaneous symmetry breaking and a nonzero average velocity in the limit  $\rho_b \rightarrow \infty$  (Kim *et al.*, 2023). We note that, for hard tracers in  $d > 1$ , a related effect—termed “swim thinning” (Burkholder and Brady, 2019)—was reported: the friction experienced by the tracer is reduced by the active bath (Burkholder and Brady, 2019; Jayaram and Speck, 2023; Knežević *et al.*, 2021; Peng and Brady, 2022) but negative frictions have not been reported so far in this case.

### 3. Beyond the Markovian approximation

It is well known that some care has to be taken when using a Markovian description to describe the long-time behavior of passive tracers. In particular, conservation laws lead to power-law decaying time correlation functions, which might cause the integrals, Eqs. (47)-(48), to diverge (van Beijeren, 1982). For dry scalar active systems, the conserved density  $\rho(\mathbf{r}, t)$  is diffusive and gives rise to slow hydrodynamic relaxation modes: for a system of size  $L \gg \ell_p$ , the relaxation time grows as  $\sim L^2$ . For an infinite system and a fully symmetric tracer, the long-time tails of the force autocorrelation function and of  $\gamma_{ij}$  have been derived and shown to decay as  $\sim t^{-(d/2+1)}$  (Feng and Hou, 2023; Granek *et al.*, 2022; Solon and Horowitz, 2022), identical to the case of a tracer in passive diffusive bath (van Beijeren, 1982; Hanna *et al.*, 1981; Spohn, 1980). Then, the Green-Kubo integrals in Eqs. (47)-(48) converge in any dimension, and the long-time diffusive behavior is unaffected.

Real tracers, however, always carry some degree of asymmetry, which leads to very different behaviors. The underlying reason is that the fluctuating force  $\mathbf{f}(t)$  is nonzero on average, as discussed in Sec. IV.A. Indeed, in the adiabatic limit,  $\langle \mathbf{f}(t) \rangle = -\mathbf{p}$ , which endows the tracer with an effective self-propulsion. Such dynamical rectification of random motion was first observed numerically in (Angelani and Di Leonardo, 2010) (see Fig. 12(b)) and later observed experimentally—in a wet system—(Kaiser *et al.*, 2014). Recently, progress has been made in modeling the motion of asymmetric tracers (Granek *et al.*, 2022; Knežević and Stark, 2020).

The asymmetric tracer’s dynamics has been derived from first principles in  $d = 1$  (Granek *et al.*, 2022), where Eq. (43) continues to hold within an adiabatic expansion. Contrary to the case of the symmetric tracer, where the long-time tails  $\sim t^{-3/2}$  lead to finite Green-Kubo integrals and effective long-time diffusion, the asymmetry shifts the decay to (Granek, 2023; Granek *et al.*, 2022)

$$\langle f(t)f(0) \rangle_c = \frac{p^2}{\rho_b(4\pi D_{\text{eff}}t)^{1/2}} + \mathcal{O}(t^{-3/2}), \quad (50)$$

$$\gamma(t) = \beta_{\text{eff}} \langle f(t)f(0) \rangle_c + \mathcal{O}(t^{-3/2}), \quad (51)$$

rendering the Green-Kubo integrals infinite in  $d = 1$ . As long as the adiabatic approximation holds, one then predicts a superdiffusive behavior with

$$\langle X^2(t) \rangle_c \sim \frac{4p^2}{3\rho_b\Gamma_{\text{th}}^2\sqrt{\pi D_{\text{eff}}}}t^{3/2}, \quad (52)$$

which is illustrated in Fig. 12(c). Likewise, the divergence in Eq. (47) is manifested in an apparent growth of the friction coefficient, measured from the average force required to tow the tracer at a constant velocity, as

$$\Gamma(t) \sim \frac{\mu p^2}{\rho_b D_{\text{eff}}} \left( \frac{t}{\pi D_{\text{eff}}} \right)^{1/2}. \quad (53)$$

These anomalous properties demonstrate that ratchet effects may induce a shift in the dynamical exponents caused by hydrodynamic modes.

Despite the theoretical advancement in the understanding of passive tracer dynamics, various open questions remain unanswered. For instance, the long-time tails in Eqs. (50)-(51) are expected to yield logarithmic corrections to the diffusion of an asymmetric tracer in  $d = 2$ , a phenomenon yet to be confirmed. Most importantly, exploring the dynamics in a controlled setting beyond the adiabatic limit remains an outstanding technical challenge.

### E. Coupled dynamics of passive tracers: Non-reciprocal interactions and localization

When several mobile tracers are embedded in an active bath, their long-range interactions, described in Sec. IV.C, lead to interesting dynamical effects. Here we show how the non-reciprocal interactions between the tracers lead to phase transitions and how the interaction between a tracer and its boundary-induced image leads to a localization transition.

Consider pinned asymmetric objects, each free to rotate along a fixed axis (see Fig. 11). The density and current modulations induced by the obstacles generate torques on each other, leading to a Kuramoto-like dynamics of their orientations (Baek *et al.*, 2018). Analysis of this dynamics has shown a transition between a phase where the obstacles' orientations are locked and one in which they rotate in synchrony. While, for the two-obstacle case studied in (Baek *et al.*, 2018), one observes a smooth crossover between these regimes, the many-body generalization studied in (Fruchart *et al.*, 2021) leads to *bona fide* phase transitions (see Fig. 13(a)). Unpinning the two rotors was also shown to generate traveling bound states (Baek *et al.*, 2018). Similar bound states were subsequently found for active particles in passive mass-conserving baths (Dolai *et al.*, 2022). It remains an interesting open question whether the many-body generalization of such states can lead to flocking/anti-flocking, as was predicted by a non-reciprocal Vicsek model (Fruchart *et al.*, 2021) and a non-reciprocal active Ising model (Martin *et al.*, 2023).

Another interesting consequence of the non-reciprocal mediated interaction can be observed for a *single* asymmetric tracer in a spherical cavity (see Fig. 13(b-c)). In this case, the generalized method of images described in Section IV.B determines the density and current modulations as the sum of contributions from the original tracer and its image upon a spherical inversion (Ben Dor *et al.*, 2022a). The non-reciprocal interactions between the object and its image lead to a transition from a steady-state distribution localized at the cavity wall to a distribution localized at its center. We stress that such a phenomenon

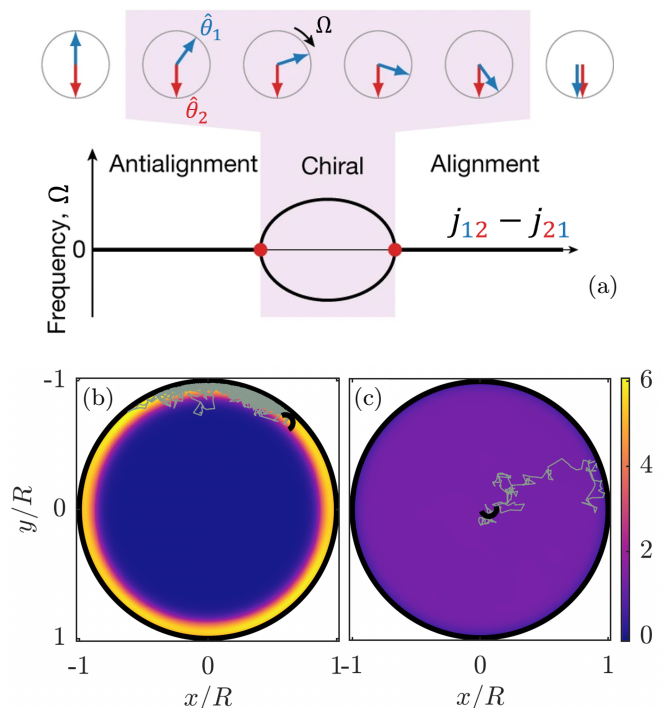


FIG. 13 (a) Non-reciprocal phase transitions. The non-reciprocal torque  $\mathbf{n}_{12} = n_{12}\hat{\mathbf{z}}$  leads to an effective Kuramoto coupling  $j_{12}\epsilon_{12} \propto n_{12}$ , where  $\epsilon_{ij}$  is the Levi-Civita symbol. The coupling asymmetry  $j_{12} - j_{21}$  determines the steady-state frequency  $\Omega$  and relative phase of  $N \gg 1$  identical copies of rotors 1 and 2. When  $\Omega \neq 0$ ,  $PT$ -symmetry is spontaneously broken. Reproduced with permission from (Fruchart *et al.*, 2021). (b-c) Localization transition of an asymmetric obstacle in a spherical cavity. Probability density and typical trajectories of a passive tracer in the active bath. Rotational friction is set to  $\Gamma_r = 10^{-2}$  (b) and  $\Gamma_r = 10^{-5}$  (c). Particle speed:  $v = 10^{-2}$ . All other parameters are set to unity. Reproduced with permission from (Ben Dor *et al.*, 2022a).

is yet another signature of how different passive and active fluids are. In a dilute passive diffusive fluid, an object cannot experience any net force in a homogeneous system. To linear order, the sole force  $\mathbf{f}$  it can experience is indeed proportional to  $\nabla\rho$ . Consequently, in the steady state,  $\nabla \cdot \mathbf{f} \propto \nabla^2\rho = 0$  since the fluid is diffusive. In analogy to Earnshaw's theorem in electrostatics, this rules out the possibility of a stable equilibrium for an object immersed in a passive diffusive fluid (Ben Dor *et al.*, 2022a; Rohwer *et al.*, 2020). Again, activity thus leads to a completely different physics.

## V. BULK DISORDER

As discussed in Section IV, localized obstacles have a far-reaching impact on the properties of active fluids. When organized coherently, they can, for instance, act as pumps and generate large-scale flows or density gradi-



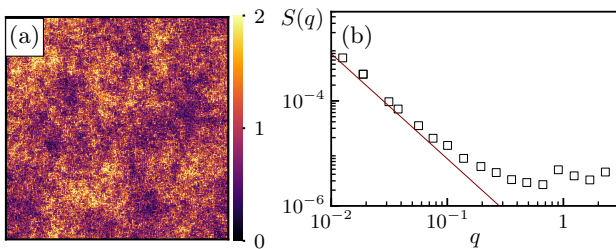


FIG. 14 Noninteracting active particles in the presence of a disordered potential. **(a)** Snapshot of the density field normalized by its average value  $\rho(\mathbf{r})/\rho_0$ . **(b)** Structure factor (symbols) compared to  $q^{-2}$  (red line), as predicted in Eq. (56). The results are obtained with RTPs on lattices with  $v = 4$ ,  $\alpha = 1$ , and the disorder potential is constructed by filling the space with square ramps with the size  $\ell = 5$  and the height  $\Delta V = 3.8$  in random locations and orientations.

ents (see Fig. 10). Naturally, this raises the question as to whether *disordered* assemblies of obstacles can also impact the properties of active fluids. In this colloquium, we discuss the case of a quenched potential disorder, which corresponds to the evolution of a system under a fixed realization of a random potential.

For equilibrium systems, this question has attracted considerable interest and many studies have been dedicated to the static and dynamical properties of passive systems in the presence of random potentials (Aharony *et al.*, 1976; Belanger *et al.*, 1983; Bricmont and Kupiainen, 1987; Fisher *et al.*, 1984; Glaus, 1986; Imbrie, 1984; Imry and Ma, 1975). Let us first briefly review the results obtained in the passive case before turning to the recent work on disordered scalar active matter. To characterize the impact of disorder on a scalar system, it is natural to consider density-density correlations, which are encoded in the structure factor. In experiments, the structure factor can be measured using scattering probes. For a system defined on a lattice of  $N$  sites, it is computed as

$$\overline{S(\mathbf{q})} \equiv \frac{1}{N} \sum_{\mathbf{r}} \overline{\langle \phi(\mathbf{r})\phi(0) \rangle} e^{i\mathbf{q}\cdot\mathbf{r}}, \quad (54)$$

where  $\phi(\mathbf{r}) \equiv \rho(\mathbf{r}) - \rho_0$  measures density fluctuations, brackets stand for steady-state averages in a particular realization of disorder, and the overline for an average over disorder realizations. In the ‘high-temperature’ homogeneous phase, the impact of disorder can be computed using a Landau-Ginzburg field theory, which leads to the addition of a squared-Lorentzian form to the result in the absence of disorder (Glaus, 1986; Kardar, 2007)

$$\overline{S(\mathbf{q})} \propto \frac{1}{(\mathbf{q}^2 + \ell_c^{-2})^2}, \quad (55)$$

where  $\ell_c$  is the correlation length of the density field. A natural question is then whether impurities can impact the existence of the ordered state and the nature of the phase transition. The first question was addressed

by Imry and Ma some 50 years ago (Imry and Ma, 1975), who showed that the lower critical dimension below which the system does not admit an ordered phase is  $d_c = 2$ . Moreover, Aizenman and Wehr showed that the system is also disordered at the marginal dimension of  $d = 2$  (Aizenman and Wehr, 1989). This is illustrated in Fig. 15(a-b), where the ordered phase is destroyed by impurities and exhibits short-range correlations.

The active case is markedly distinct: In the homogeneous phase, the disorder leads to a scale-free steady state with a structure factor that diverges as (Ro *et al.*, 2021)

$$\overline{S(\mathbf{q})} \underset{q \rightarrow 0}{\propto} \frac{1}{\mathbf{q}^2}. \quad (56)$$

As shown in Fig. 14, fluctuations at small  $q$  are strongly enhanced compared to the passive case: The correlation length is infinite and density-density correlations decay as  $\langle \phi(\mathbf{r})\phi(0) \rangle \propto r^{2-d}$  for  $d > 2$ , and logarithmically in  $d = 2$ .

Beyond creating a long-range correlated fluid, disorder also has a strong impact on the existence of a long-range ordered phase. For a system undergoing MIPS, disorder prevents phase separation in both 2 and 3 dimensions. Compared to the passive case, the lower critical dimension is increased from  $d_c = 2$  to  $d_c = 4$ . As shown in Fig. 15(c-d), the phase-separated state is replaced by a frozen scale-free distribution with large-amplitude density fluctuations.

### A. A simple physical picture

To understand the difference between the active and passive cases, let us first recall the results of Sec. IV. At the microscopic scale, a random potential is generically asymmetric and thus, acting as a pump, it generates a ratchet current. As we now argue, the net effect of a dilute collection of randomly placed pumps is to generate density-density fluctuations consistent with Eq. (56) as depicted in Fig. 16.

To see this explicitly, consider a dilute distribution of pumps whose force density we denote by  $\mathbf{f}(\mathbf{r})$ . Each pump acts as a current source that modifies the density according to Eq. (36). The contributions from the pumps add up independently, resulting in the overall density modulation given by

$$\langle \phi(\mathbf{r}) \rangle = \beta_{\text{eff}} \int d^d \mathbf{r}' \mathbf{f}(\mathbf{r}') \cdot \nabla_{\mathbf{r}} G(\mathbf{r} - \mathbf{r}'), \quad (57)$$

where  $G(\mathbf{r} - \mathbf{r}') = G(\mathbf{r}, \mathbf{r}')$  is the Green’s function of the Laplacian. Note that for a single pump,  $\mathbf{f}(\mathbf{r}) = \mathbf{p}\delta^d(\mathbf{r} - \mathbf{r}_0)$ , Eq. (57) gives back the solution Eq. (34) derived in Sec. IV.A for an isolated asymmetric inclusion. In

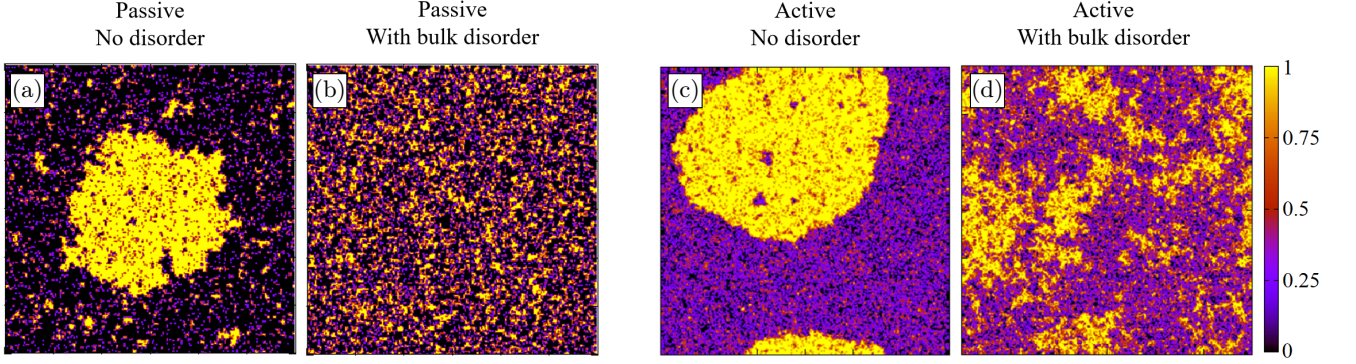


FIG. 15 Comparison between equilibrium and active systems undergoing phase separation. A passive lattice gas with attractive interaction (a), and an active lattice gas with repulsive interactions (c), may both experience bulk phase separation. When a random potential is added to the passive system, the phase separation is suppressed, leading to a homogeneous phase with short-range correlations (b). In the active case (d), a scale-free distribution of particles replaces the bulk phase separation. Color encodes density. Reproduced with permission from (Ro *et al.*, 2021).

Fourier space, the convolution in Eq. (57) takes the form<sup>3</sup>

$$\langle \phi(\mathbf{q}) \rangle = \beta_{\text{eff}} L^{d/2} i\mathbf{q} \cdot \mathbf{f}(\mathbf{q}) G(\mathbf{q}) ,$$

where  $G(\mathbf{q}) = -L^{-d/2} q^{-2}$ ,  $q = |\mathbf{q}|$  and  $L$  is the system size. Assuming Gaussian-distributed uncorrelated pumps with a typical strength  $\chi$ ,  $\mathbf{f}(\mathbf{q})$  is entirely characterized by

$$\begin{aligned} \overline{f_i(\mathbf{q})} &= 0 , \\ \overline{f_i(\mathbf{q}) f_j(\mathbf{q}')} &= \chi^2 \delta_{ij} \delta_{\mathbf{q}, -\mathbf{q}'} . \end{aligned}$$

For noninteracting particles, the structure factor satisfies

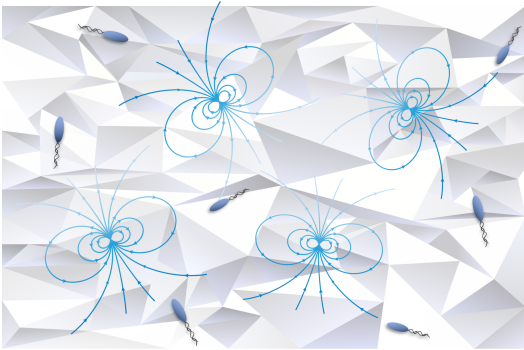


FIG. 16 Schematic depiction of disorder acting as a random array of pumps for active particles, leading to a dipolar flow field.

<sup>3</sup> In what follows we use the Fourier convention:  $f(\mathbf{q}) = L^{-d/2} \int d^d \mathbf{r} e^{-i\mathbf{q} \cdot \mathbf{r}} f(\mathbf{r})$  and  $f(\mathbf{r}) = L^{-d/2} \sum_{\mathbf{q}} e^{i\mathbf{q} \cdot \mathbf{r}} f(\mathbf{q})$

$\overline{\langle \phi(\mathbf{q}) \phi(-\mathbf{q}) \rangle} = \overline{\langle \phi(\mathbf{q}) \rangle \langle \phi(-\mathbf{q}) \rangle}$  so that

$$\begin{aligned} \overline{\langle \phi(\mathbf{q}) \phi(-\mathbf{q}) \rangle} &= \frac{\beta_{\text{eff}}^2}{q^4} \sum_{i,j=1}^d q_i q_j \overline{f_i(\mathbf{q}) f_j(-\mathbf{q})} \\ &= \frac{\beta_{\text{eff}}^2 \chi^2}{q^2} , \end{aligned} \quad (58)$$

which is indeed compatible with the 2d structure factor presented in Fig. 14.

## B. Field-theoretical description

In order to account for the effects of interactions between the particles, it is useful to introduce a field-theoretical description by building up on the insights of the previous section. Since the quenched random potential translates, through the ratchet effect, into a quenched random forcing, one can start with a simple linear field theory of the form:

$$\frac{\partial}{\partial t} \phi(\mathbf{r}, t) = -\nabla \cdot \mathbf{j}(\mathbf{r}, t) , \quad (59)$$

$$\mathbf{j}(\mathbf{r}, t) = -\nabla u[\phi] + \mathbf{f}(\mathbf{r}) + \sqrt{2D} \boldsymbol{\eta}(\mathbf{r}, t) , \quad (60)$$

where  $\phi(\mathbf{r}, t)$  describes the coarse-grained density fluctuations,  $\mathbf{j}(\mathbf{r}, t)$  is the associated current, and  $\boldsymbol{\eta}(\mathbf{r}, t)$  is a centered Gaussian white noise field such that  $\langle \eta_i(\mathbf{r}, t) \eta_j(\mathbf{r}', t') \rangle = \delta_{ij} \delta(t-t') \delta(\mathbf{r}-\mathbf{r}')$ . The mobility is set to one and, similar to the previous section, the force density satisfies  $\overline{f_i(\mathbf{r})} = 0$  and  $\overline{f_i(\mathbf{r}) f_j(\mathbf{r}')} = \sigma^2 \delta_{ij} \delta^d(\mathbf{r}-\mathbf{r}')$ . At linear level in  $\phi$  and to leading order in a gradient expansion, the effective chemical potential  $u$  is of the form

$$u[\phi(\mathbf{r}, t)] = u\phi(\mathbf{r}, t) - K \nabla^2 \phi(\mathbf{r}, t) , \quad (61)$$

with  $u, K > 0$  to ensure stability.

Before proceeding, let us highlight the difference between the current induced by the force density  $\mathbf{f}(\mathbf{r})$  and the Brownian noise  $\boldsymbol{\eta}(\mathbf{r}, t)$ . To do so, we consider the time-averaged total current, denoted as

$$\mathcal{J} = \frac{1}{\Delta t} \int_0^{\Delta t} dt \int d^d \mathbf{r} \mathbf{j}(\mathbf{r}, t), \quad (62)$$

flowing through the whole system during the time interval  $\Delta t$  in the presence of disorder and periodic boundary conditions. The magnitude of  $\mathcal{J}$  can be characterized by averaging  $\mathcal{J}^2$  over both noise and disorder. Direct algebra shows that this second moment is given by

$$\overline{\langle \mathcal{J}^2 \rangle} = d\sigma^2 L^d + 2dDL^d \Delta t^{-1}. \quad (63)$$

Equation (63) demonstrates that although the scaling with the system size is the same for both the random force and noise-induced terms, the scaling with the time interval is drastically different. The quenched random force induces a net stationary current, which remains finite as  $\Delta t \rightarrow \infty$ . By contrast, the current fluctuations induced by the Brownian noise decay as  $\Delta t^{-1}$  once averaged over the time interval  $\Delta t$ . To verify this prediction, we measure  $\mathcal{J}$  by simulating RTPs with and without disorder, subject to periodic boundary conditions. The scaling of the second moment with the system size shown in Fig. 17(a) indeed confirms Eq. (63). In Fig. 17(b), we also show how the second moment scales with the observation time interval, both with and without disorder. In the absence of disorder,  $\mathcal{J}$  is dominated by the time-dependent noise, and its second moment indeed shows a diffusive scaling  $\overline{\langle \mathcal{J}^2 \rangle} \propto \Delta t^{-1}$  (red symbols). In the presence of disorder, the ballistic contribution of the random force dominates the long-time scaling, as confirmed by our simulation (blue symbols).

Let us now turn to the discussion of the density-density correlations. A direct computation using Eqs. (59)-(61) shows that the structure factor of the (linearised) theory

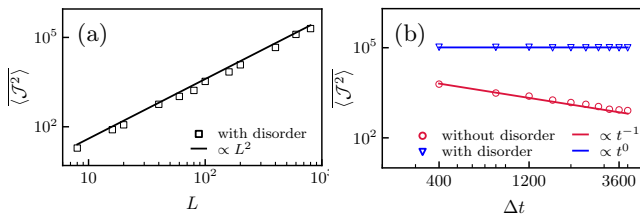


FIG. 17 Scaling of the time-averaged total current with respect to, (a) system size and, (b) the measurement time interval. The second moment  $\overline{\langle \mathcal{J}^2 \rangle}$  measured in simulation (symbols) is compared to the scaling trends predicted in Eq. (63) (solid lines). Parameters:  $d = 2$ , particle speed  $v = 4$ , the amplitude of the random potential  $\Delta V = 3.8$ ,  $\Delta t = 4000$  in (a),  $L = 800$  in (b), and averaged over 50 realizations of disorder.

is given by:

$$S(\mathbf{q}) = \frac{\sigma^2}{q^2(u + Kq^2)^2} + \frac{D}{(u + Kq^2)}. \quad (64)$$

We note that Eqs. (64) and (58) predict the same small- $q$  behavior upon identifying  $\sigma/u$  with  $\chi\beta_{\text{eff}}$ . To check the relevance of non-linearities, terms of the form  $s\phi^n(\mathbf{r}, t)$  can be added to the effective chemical potential  $\mathbf{u}$ , and their relevance can be accessed under diffusive scaling  $\mathbf{r} \rightarrow b\mathbf{r}$  and  $t \rightarrow b^2t$  in Eqs. (59)-(60). First, since the structure factor satisfies  $\phi(\mathbf{q})\phi(\mathbf{q}') \propto q^{-2}\delta^d(\mathbf{q} + \mathbf{q}')$ , the density modulations in real space are rescaled as  $\phi \rightarrow b^{1-d/2}\phi$ . Accordingly, any non-linear term transforms as  $\phi^n \rightarrow b^{n(1-d/2)}\phi^n$ , and they are irrelevant for  $d > 2$ . The case  $d = 2$  is marginal, and it was shown in (Ro *et al.*, 2021) that the theory is self-consistent up to length scales such that  $\ell \ll \ell^*$  with  $\ell^* \equiv a \exp(\pi u^2 \rho_b^2 / \sigma^2)$ . Beyond such length scales, that have never been explored numerically, a different behavior for  $S(\mathbf{q})$  may emerge.

We now discuss how a generalization of the Imry-Ma argument predicts the destruction of an ordered phase in dimensions below the lower critical dimension of  $d_c = 4$ . First, using a Helmholtz-Hodge decomposition, we write the random force field as <sup>4</sup>

$$\mathbf{f}(\mathbf{r}) = -\nabla U(\mathbf{r}) + \boldsymbol{\Xi}(\mathbf{r}), \quad (65)$$

where  $U(\mathbf{r})$  is an *effective potential* that differs from  $V(\mathbf{r})$  and the vector field  $\boldsymbol{\Xi}(\mathbf{r})$  satisfies  $\nabla \cdot \boldsymbol{\Xi}(\mathbf{r}) = 0$ . We note that  $\boldsymbol{\Xi}$  impacts the current but not the dynamics of the density field or its distribution. The statistics of  $\mathbf{f}(\mathbf{r})$  imply that

$$\overline{U(\mathbf{q})U(\mathbf{q}')} = \sigma^2 q^{-2} \delta_{\mathbf{q}, -\mathbf{q}}^d, \quad (66)$$

$$\overline{\Xi_i(\mathbf{q})\Xi_j(\mathbf{q}')} = \sigma^2 (\delta_{ij} - q_i q_j / q^2) \delta_{\mathbf{q}, -\mathbf{q}}^d, \quad (67)$$

$$\overline{U(\mathbf{q})\boldsymbol{\Xi}(\mathbf{q}')} = 0. \quad (68)$$

Because we are considering a linear theory and  $\boldsymbol{\Xi}$  is divergence-free, the dynamics of the density field is equivalent to an equilibrium dynamics in a potential  $U(\mathbf{r})$  (Ao, 2004; Kwon *et al.*, 2005). Inspection of Eq. (66) shows that  $U(\mathbf{r})$  behaves like a Gaussian free field, equivalent to a random surface in  $d = 2$ . Its deep and scale-free minima account for the long-range correlations experienced by the density field. Furthermore, we can now predict the lower critical dimension by applying the standard Imry-Ma argument to an equilibrium dynamics in the presence of the potential  $U(\mathbf{r})$  (Aharony *et al.*, 1976;

<sup>4</sup> In the reported simulations, periodic boundary conditions were employed and the Helmholtz-Hodge decomposition also includes harmonic functions that are linear combinations of constant flows along the system axes. They do not impact the discussion of the generalized Imry Ma argument.

Imry and Ma, 1975). This entails comparing the surface energy cost of overturning an ordered domain of linear size  $\ell$ —given by  $\gamma\ell^{d-1}$  with  $\gamma$  a surface-tension-like coefficient—to the bulk energy gain of the domain due to a locally favorable disorder potential. The latter, given by  $E(\ell) = \int_{\ell^d} d^d\mathbf{r}' \rho_0 U(\mathbf{r}')$ , has a typical value of  $E(\ell) \propto \sigma\rho_0\ell^{1+d/2}$ , estimated by noting that the variance satisfies  $\overline{E(\ell)^2} = \sigma^2\rho_0^2\ell^{d+2}$ . For  $d < 4$ , the surface energy cost is negligible on large enough length scales, and the system cannot phase-separate into macroscopic domains.

We note that the field theory studied in Eqs. (57)-(60) is equivalent to that describing passive particles in a random force field. At the single-particle level, this system has attracted some attention in the past (Bouchaud *et al.*, 1990; Derrida, 1983; Derrida and Pomeau, 1982; Fisher, 1984; Sinai, 1983) and the analysis above extends these works to the many-body case. We note that, for active particles in a random potential, the one-dimensional dynamics can be shown to be equivalent to a Sinai random walk (Ben Dor *et al.*, 2019). In higher dimensions, the dynamics remains to be studied.

## VI. BOUNDARY DISORDER.

In equilibrium, boundaries and boundary conditions generically do not alter bulk phase behaviors, due to the subextensive nature of their contributions to the free energy. This is illustrated in Fig. 18, where replacing flat confining walls with rough ones has no impact on bulk phase separation. An important consequence is that, in simulations or theoretical analysis, convenient boundary conditions (open or periodic) are often used to study bulk properties in equilibrium statistical mechanics.

Rough boundary conditions can be implemented (as described earlier) through a wall potential  $V(x, \mathbf{r}_{\parallel})$ , where  $x$  is the coordinate normal to the wall and  $\mathbf{r}_{\parallel}$  is a  $(d-1)$ -dimensional vector parallel to the wall. For example,  $V(x, \mathbf{r}_{\parallel})$  can be modeled by setting  $V(x < 0, \mathbf{r}_{\parallel}) = \infty$  and placing wedge-shaped asymmetric obstacles along the wall whose orientations are chosen randomly (see Figs. 18(b) and 19(b) for a qualitative illustration). The obstacles then have a finite extent  $x_w$  in the  $\hat{\mathbf{x}}$  direction.

Figure 19 then shows a striking difference with the passive case: the rough ‘disordered’ walls destroy bulk phase separation, leading to a nontrivial density distribution. This was shown to hold even in the macroscopic limit where the boundaries are sent to infinity. It shows that, even in the thermodynamic limit, the bulk behaviors of active systems with closed or periodic boundary conditions can be markedly different (Ben Dor *et al.*, 2022b), in stark contrast with passive systems (away from critical points). As we now discuss, the far-field density modulations and currents induced by such a disordered wall and their effects on the bulk behavior can be computed by modeling the disordered wall as a collection of force

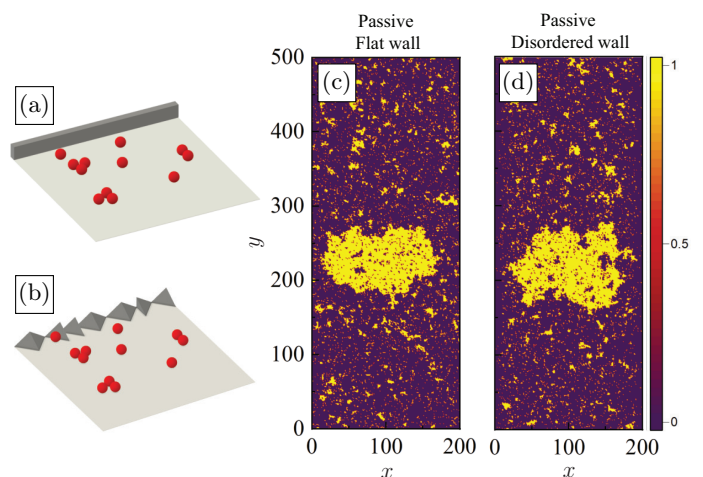


FIG. 18 Impact of flat (a) and disordered (b) walls on phase separation in passive systems. In the presence of attractive interactions between the particles, simulations of a passive lattice gas at low temperature show phase separation in both settings (panels c and d). Color encodes density. Reproduced with permission from (Ben Dor *et al.*, 2022b).

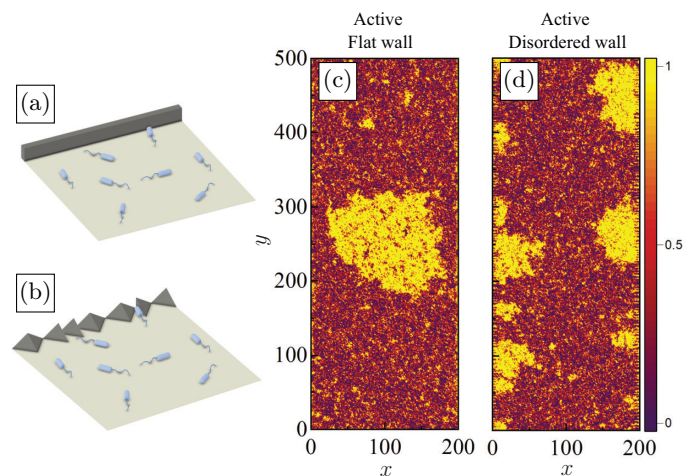


FIG. 19 Impact of flat (a) and disordered (b) walls on phase separation in active systems. In contrast to the passive case shown in Fig. 18, simulations of an active lattice gas (d) show that the disordered boundary destroys the phase separation observed in the presence of a flat wall (c), leading to a scale-free distribution of particles. Color encodes density. Reproduced with permission from (Ben Dor *et al.*, 2022b).

monopoles randomly placed at  $x = 0$  and oriented along the  $\mathbf{r}_{\parallel}$  surface.

### A. A simple physical picture

Again, we start by considering the dilute case and describe the force monopoles using a quenched Gaussian

random force density,  $\mathbf{f}(\mathbf{r}_{\parallel}, x)$ , whose statistics satisfy:

$$\begin{aligned} \overline{f_i(\mathbf{r}_{\parallel}, x)} &= 0, \\ \overline{f_i(\mathbf{r}_{\parallel}, x) f_j(\mathbf{r}'_{\parallel}, x')} &= 2\chi^2 \delta_{ij}^{\parallel} \delta(x) \delta(x') \delta^{(d-1)}(\mathbf{r}_{\parallel} - \mathbf{r}'_{\parallel}), \end{aligned} \quad (69)$$

where  $\chi$  sets the scale of the force density,  $\delta_{ij}^{\parallel} = 1$  if  $i = j \neq x$  and  $\delta_{ij}^{\parallel} = 0$  otherwise. Similar to the bulk disorder case, the density modulations in the system satisfy

$$\langle \phi(\mathbf{r}) \rangle = \beta_{\text{eff}} \int d^d \mathbf{r}' \mathbf{f}(\mathbf{r}') \cdot \nabla_{\mathbf{r}} G_{\text{w}}(\mathbf{r}, \mathbf{r}'), \quad (70)$$

but this time  $G_{\text{w}}(\mathbf{r}, \mathbf{r}')$  is the Green's function associated with a Poisson equation in a half-infinite system with Neumann boundary conditions at  $x = 0$ , see Sec. IV.B. Using this, one finds that the two-point correlation function satisfies (Ben Dor *et al.*, 2022b):

$$\overline{\langle \phi(x, \mathbf{r}_{\parallel}) \phi(x', \mathbf{r}'_{\parallel}) \rangle} = \frac{2\beta_{\text{eff}} \chi (x + x')}{S_d [(x + x')^2 + |\Delta \mathbf{r}_{\parallel}|^2]^{\frac{d}{2}}}, \quad (71)$$

with  $S_d$  the  $d$ -dimensional solid angle and  $\Delta \mathbf{r}_{\parallel} = \mathbf{r}_{\parallel} - \mathbf{r}'_{\parallel}$ . This equation shows that there are large-scale density modulations that decay in amplitude but increase in range as one looks further from the wall.

The heuristic prediction Eq. (71) is verified numerically in Fig. 20 using microscopic simulations of non-interacting particles in two space dimensions. To do so, the prediction Eq. (71) for  $x = x'$  can be rewritten as:

$$\frac{\overline{\langle \phi(x, y) \phi(x, y + \Delta y) \rangle}}{\overline{\langle \phi(x, y) \phi(x, y) \rangle}} = \frac{1}{1 + \left(\frac{\Delta y}{2x}\right)^2} \equiv \mathcal{S}\left(\frac{\Delta y}{x}\right), \quad (72)$$

which highlights that the correlations along  $y$  increase linearly with the distance  $x$  to the wall.

An illuminating way to understand these results is to consider the currents generated in the system: the ratchet mechanism generates local currents in the active fluid next to the wall. Since the number of particles is conserved, this microscopic stirring develops into large-scale eddies in the bulk. In fact, on large scales, the current can be estimated as  $\mathbf{J}(x, \mathbf{r}_{\parallel}) \approx -D_{\text{eff}} \nabla \phi(x, \mathbf{r}_{\parallel})$ , leading to:

$$\begin{aligned} \overline{\langle \mathbf{J}(x, \mathbf{q}_{\parallel}) \cdot \mathbf{J}^*(x, \mathbf{k}_{\parallel}) \rangle} &= 2^d d (\mu \chi)^2 |\mathbf{q}_{\parallel}|^2 e^{-2|\mathbf{q}_{\parallel}|x} \\ &\times \pi^{d-1} \delta^{(d-1)}(\mathbf{q}_{\parallel} + \mathbf{k}_{\parallel}). \end{aligned} \quad (73)$$

The current-current correlations first increase for small  $|\mathbf{q}_{\parallel}|$  and are then exponentially suppressed for  $|\mathbf{q}_{\parallel}| > x^{-1}$ : like the density-density correlations, the eddies have a transverse extent that grows linearly with the distance  $x$  to the wall, as verified in Fig. 21 using a scaling form similar to that of Eq. (72).

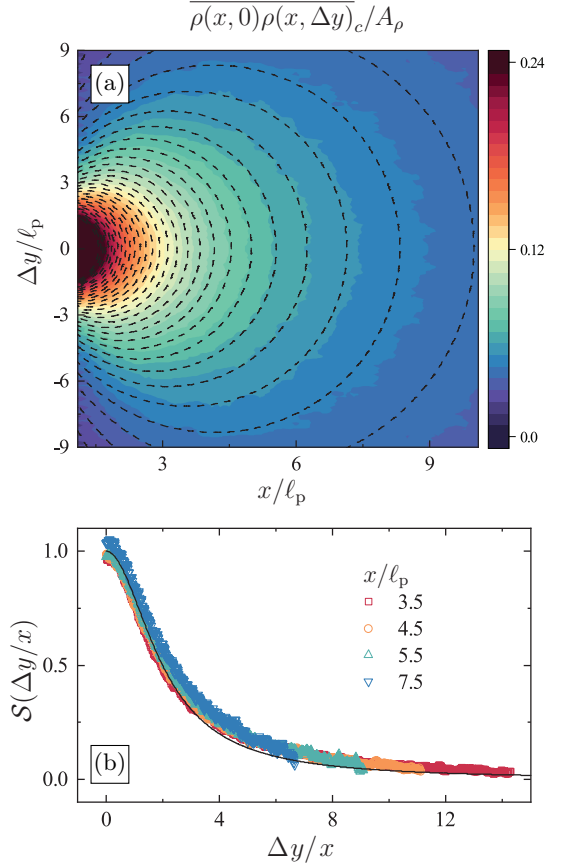


FIG. 20 Disorder-averaged two-point density correlation function of non-interacting RTPs in two dimensions in the presence of a disordered wall at  $x = 0$ . (a) The two-point correlation function as  $x$  and  $\Delta y$  are varied, calculated from simulations, is shown by the color map. The value of  $A_{\rho} \equiv \ell_p S_d^{-1} (2\beta_{\text{eff}} \chi)^2$  is obtained from a fit of the data to Eq. (71). The theoretical prediction of Eq. (71) is then used to produce dashed contour lines that match the levels of the color bar. Both theory and simulations are normalized by  $A_{\rho}$ . (b) A verification of the scaling form Eq. (72) for the density-density correlation function. The data shown in panel (a) for four different distances  $x$  from the wall are collapsed onto a single curve, as predicted. Reproduced with permission from (Ben Dor *et al.*, 2022b).

## B. Linear field theory

To account for interactions, it is useful to follow Sec. V.B and use the linear field theory Eqs. (59)-(60) to describe the evolution of the density fluctuations  $\phi(\mathbf{r}, t)$ . This time, however, the statistics of the random force field  $\mathbf{f}(\mathbf{r})$  satisfy

$$f_x(x, \mathbf{r}_{\parallel}) = 0, \quad (74)$$

$$f_i(x, \mathbf{r}_{\parallel}) = 0, \quad (75)$$

$$\overline{f_i(x, \mathbf{r}_{\parallel}) f_j(x', \mathbf{r}'_{\parallel})} = 2\sigma^2 \delta_{ij} \delta(x) \delta(x') \delta^{(d-1)}(\mathbf{r}_{\parallel} - \mathbf{r}'_{\parallel}),$$

where  $i$  and  $j$  label directions parallel to the wall. The amplitude  $\sigma$  of the random force density depends on the

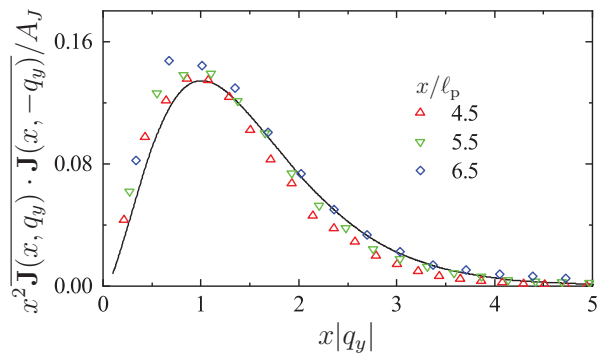


FIG. 21 Fourier transform along the  $\hat{y}$  direction of the current-current correlation function measured at a distance  $x$  from the wall and averaged over disorder. The data are obtained for three values of  $x$  and normalized by a factor  $A_J \equiv 2d(2\pi)^{d-1}(\mu\chi)^2$ . As predicted by the theory, the data can be collapsed onto a single curve, corresponding to Eq. (73), by properly scaling the abscissa and the ordinates. Reproduced with permission from (Ben Dor *et al.*, 2022b).

average bulk density  $\rho_b$  but is, to leading order, independent of  $\phi$ . Direct algebra shows that this linear field theory predicts density modulations and currents compatible with the prediction Eqs. (72) and (73) on large length scales upon identifying  $2\chi\beta_{\text{eff}} = \sigma/u$ .

The self-consistency of the linear theory can be checked using a scaling argument similar to what was done for the bulk disorder in Sec. V.B. This time, non-linearities are found to be irrelevant for  $d > 1$ . We now discuss how the field theory allows estimating the impact of boundary disorder on bulk phase separation in active fluids.

### C. The effect of disordered boundaries on MIPS

Again, one uses the Helmholtz-Hodge decomposition Eq. (65) of the random forcing to identify an effective potential  $U(\mathbf{r})$ . Since, the effective potential satisfies  $\nabla^2 U(\mathbf{r}) = -\nabla \cdot \mathbf{f}(\mathbf{r})$ , Eqs. (74)-(75) imply that the statistics of  $U$  obey

$$\overline{U(\mathbf{r})} = 0, \quad (76)$$

$$\overline{U(\mathbf{r})U(\mathbf{r}')} = \frac{\sigma^2}{S_d} \frac{(x+x')}{[(x+x')^2 + |\Delta\mathbf{r}_{\parallel}|^2]^{d/2}}. \quad (77)$$

This can then be used to compare the surface energy  $\gamma\ell^{d-1}$  of an ordered droplet of linear size  $\ell$  to its bulk energy  $\int_{\ell^d} d^2\mathbf{r} U(\mathbf{r})$ . Using Eq. (77), the latter is estimated to scale as  $\ell^{(d+1)/2}$  so that the surface energy is unable to stabilize a macroscopic droplet below a lower critical dimension  $d_c = 3$ . As shown in Fig. 19, the phase-separated state is indeed replaced by scale-free density modulations in  $d = 2$ . This result highlights how boundaries can play a much more important role in active systems than in their passive counterparts.

## VII. CONCLUSION, PERSPECTIVES.

In this colloquium, we have reviewed the anomalous mechanical properties of dry scalar active systems that have attracted a lot of attention recently. We have shown how the emergence of ratchet currents and the lack of conservation of momentum lead to a wide variety of phenomena, from the lack of an equation of state for pressure to the destruction of bulk phase separation by boundary disorder, all of which can be captured within a unifying perspective. These phenomena endow active systems with properties that are strikingly different from that of passive matter, whose consequences are only starting to be explored.

Indeed, even basic concepts like surface tension are not well understood and are intensely debated (Bialké *et al.*, 2015; Fausti *et al.*, 2021; Hermann *et al.*, 2019; Lauersdorf *et al.*, 2021; Marini Bettolo Marconi *et al.*, 2016; Omar *et al.*, 2020; Paliwal *et al.*, 2017; Zakine *et al.*, 2020). Furthermore, much of the research so far has been based on theoretical studies of minimal models. How the anomalous mechanical properties can be measured or harnessed experimentally is an exciting research direction (Junot *et al.*, 2017). Similarly, the far-field density and current modulations induced by localized obstacles, as well as the scale-free state induced by bulk and boundary disorder, are within reach of modern experimental active-matter systems (Bhattacharjee and Datta, 2019; Chardac *et al.*, 2021; Takaha and Nishiguchi, 2023). Their measurement is an ongoing challenge.

Finally, in this colloquium, we have focused on dry scalar active matter to single out the interesting phenomena that are solely due to the interplay between activity and mechanical forces. Other situations, where more hydrodynamic fields are relevant, are bound to lead to even richer physics. In particular, the role of obstacles, boundaries and disorder in wet active matter, or in polar and nematic active fluids, is a current frontier in the field.

## ACKNOWLEDGMENTS

This colloquium is born out of many discussions and collaborations on the mechanical properties of scalar active systems that have involved many colleagues. In particular, we are grateful to Yongjoo Baek, Aparna Baskaran, Mike Cates, Adrian Daerr, Ydan Ben Dor, Yaouen Fily, Jordan Horowitz, Nikolai Nikola, Gianmarco Spera, Joakim Stenhammar, Ari Turner, Frédéric van Wijland, Raphaël Voituriez, Ruben Zakine, and Yongfeng Zhao. JT thanks ANR THEMA for financial support and MSC laboratory for hospitality. MK is supported by NSF grant DMR-2218849. YK, OG and SR acknowledge financial support from ISF (2038/21) and NSF/BSF (2022605). OG also acknowledges support from the Adams Fellowship Program of the Israeli

Academy of Science and Humanities.

## REFERENCES

- Adachi, Kyosuke, and Kyogo Kawaguchi (2020), “Universality of active and passive phase separation in a lattice model,” arXiv:2012.02517 [cond-mat.stat-mech].
- Agranov, Tal, Sunghan Ro, Yariv Kafri, and Vivien Lecomte (2021), “Exact fluctuating hydrodynamics of active lattice gases—typical fluctuations,” *J. Stat. Mech. Theory Exp.* **2021** (8), 083208.
- Aharony, Amnon, Yoseph Imry, and Shang-keng Ma (1976), “Lowering of Dimensionality in Phase Transitions with Random Fields,” *Phys. Rev. Lett.* **37** (20), 1364–1367.
- Ai, Bao-Quan, and Jian-Chun Wu (2014), “Transport of active ellipsoidal particles in ratchet potentials,” *J. Chem. Phys.* **140** (9), 094103.
- Aizenman, Michael, and Jan Wehr (1989), “Rounding of first-order phase transitions in systems with quenched disorder,” *Phys. Rev. Lett.* **62** (21), 2503–2506.
- Anderson, Caleb J, Guillaume Briand, Olivier Dauchot, and Alberto Fernández-Nieves (2022), “Polymer-chain configurations in active and passive baths,” *Phys. Rev. E* **106** (6), 064606.
- Angelani, L, A. Costanzo, and R. Di Leonardo (2011), “Active ratchets,” *EPL* **96** (6), 68002.
- Angelani, Luca, and Roberto Di Leonardo (2010), “Geometrically biased random walks in bacteria-driven microshuttles,” *New J. Phys.* **12** (11), 113017.
- Angelani, Luca, Roberto Di Leonardo, and Giancarlo Ruocco (2009), “Self-starting micromotors in a bacterial bath,” *Physical review letters* **102** (4), 048104.
- Angelini, Thomas E, Edouard Hannezo, Xavier Trepast, Manuel Marquez, Jeffrey J. Fredberg, and David A. Weitz (2011), “Glass-like dynamics of collective cell migration,” *Proc. Natl. Acad. Sci.* **108** (12), 4714–4719.
- Ao, Ping (2004), “Potential in stochastic differential equations: novel construction,” *J. Phys. A: Math. Gen.* **37** (3), L25–L30.
- Baek, Yongjoo, Alexandre P. Solon, Xinpeng Xu, Nikolai Nikola, and Yariv Kafri (2018), “Generic Long-Range Interactions Between Passive Bodies in an Active Fluid,” *Phys. Rev. Lett.* **120** (5), 058002.
- Basu, Urna, Satya N. Majumdar, Alberto Rosso, Sanjib Sabhapandit, and Grégory Schehr (2020), “Exact stationary state of a run-and-tumble particle with three internal states in a harmonic trap,” *J. Phys. A: Math. Theor.* **53** (9), 09LT01.
- Bäuerle, Tobias, Andreas Fischer, Thomas Speck, and Clemens Bechinger (2018), “Self-organization of active particles by quorum sensing rules,” *Nat. Commun.* **9** (1), 3232.
- Bechinger, Clemens, Roberto Di Leonardo, Hartmut Löwen, Charles Reichhardt, Giorgio Volpe, and Giovanni Volpe (2016), “Active Particles in Complex and Crowded Environments,” *Rev. Mod. Phys.* **88** (4), 045006.
- van Beijeren, Henk (1982), “Transport properties of stochastic Lorentz models,” *Rev. Mod. Phys.* **54** (1), 195–234.
- Belanger, D P, A. R. King, V. Jaccarino, and J. L. Cardy (1983), “Random-field critical behavior of a  $d = 3$  Ising system,” *Phys. Rev. B* **28** (5), 2522–2526.
- Ben Dor, Ydan, Yariv Kafri, Mehran Kardar, and Julien Tailleur (2022a), “Passive objects in confined active fluids: A localization transition,” *Phys. Rev. E* **106** (4), 044604.
- Ben Dor, Ydan, Sunghan Ro, Yariv Kafri, Mehran Kardar, and Julien Tailleur (2022b), “Disordered boundaries destroy bulk phase separation in scalar active matter,” *Phys. Rev. E* **105** (4), 044603.
- Ben Dor, Ydan, Eric Woillez, Yariv Kafri, Mehran Kardar, and Alexandre P. Solon (2019), “Ramifications of disorder on active particles in one dimension,” *Phys. Rev. E* **100** (5), 052610.
- Berg, Howard C (2004), *E. coli in Motion* (Springer).
- Berthier, Ludovic, Elijah Flenner, and Grzegorz Szamel (2017), “How active forces influence nonequilibrium glass transitions,” *New J. Phys.* **19** (12), 125006.
- Berthier, Ludovic, Elijah Flenner, and Grzegorz Szamel (2019), “Glassy dynamics in dense systems of active particles,” *J. Chem. Phys.* **150** (20), 200901.
- Bhattacharjee, Tapomoy, and Sujit S. Datta (2019), “Bacterial hopping and trapping in porous media,” *Nat. Commun.* **10** (1), 2075.
- Bialké, Julian, Jonathan T. Siebert, Hartmut Löwen, and Thomas Speck (2015), “Negative Interfacial Tension in Phase-Separated Active Brownian Particles,” *Phys. Rev. Lett.* **115** (9), 098301.
- Bouchaud, J P, A. Comtet, A. Georges, and P. Le Doussal (1990), “Classical diffusion of a particle in a one-dimensional random force field,” *Ann. Phys. (N. Y.)* **201** (2), 285–341.
- Brenner, Michael P, Leonid S. Levitov, and Elena O. Budrene (1998), “Physical Mechanisms for Chemotactic Pattern Formation by Bacteria,” *Biophys. J.* **74** (4), 1677–1693.
- Bricard, Antoine, Jean-Baptiste Caussin, Nicolas Desreumaux, Olivier Dauchot, and Denis Bartolo (2013), “Emergence of macroscopic directed motion in populations of motile colloids,” *Nature* **503** (7474), 95–98.
- Bricmont, J, and A. Kupiainen (1987), “Lower critical dimension for the random-field Ising model,” *Phys. Rev. Lett.* **59** (16), 1829–1832.
- Burkholder, Eric W, and John F. Brady (2017), “Tracer diffusion in active suspensions,” *Phys. Rev. E* **95** (5), 052605.
- Burkholder, Eric W, and John F Brady (2019), “Fluctuation-dissipation in active matter,” *J. Chem. Phys.* **150** (18), 184901.
- Buttinoni, Ivo, Julian Bialké, Felix Kümmel, Hartmut Löwen, Clemens Bechinger, and Thomas Speck (2013), “Dynamical Clustering and Phase Separation in Suspensions of Self-Propelled Colloidal Particles,” *Phys. Rev. Lett.* **110** (23), 238301.
- Caballero, Fernando, Cesare Nardini, and Michael E. Cates (2018), “From bulk to microphase separation in scalar active matter: a perturbative renormalization group analysis,” *J. Stat. Mech. Theory Exp.* **2018** (12), 123208.
- Caporusso, Claudio B, Pasquale Digregorio, Demian Levis, Leticia F. Cugliandolo, and Giuseppe Gonnella (2020), “Motility-Induced Microphase and Macrophase Separation in a Two-Dimensional Active Brownian Particle System,” *Phys. Rev. Lett.* **125** (17), 178004.
- Cates, M E, and J. Tailleur (2013), “When are active Brownian particles and run-and-tumble particles equivalent? Consequences for motility-induced phase separation,” *EPL* **101** (2), 20010.
- Cates, Michael E, and Julien Tailleur (2015), “Motility-Induced Phase Separation,” *Annu. Rev. Condens. Matter Phys.* **6** (1), 219–244.

- Chardac, Amélie, Suraj Shankar, M. Cristina Marchetti, and Denis Bartolo (2021), “Emergence of dynamic vortex glasses in disordered polar active fluids,” *Proc. Natl. Acad. Sci.* **118** (10), e2018218118.
- Chaté, Hugues (2020), “Dry Aligning Dilute Active Matter,” *Annu. Rev. Condens. Matter Phys.* **11** (1), 189–212.
- Chen, D T N, A. W. C. Lau, L. A. Hough, M. F. Islam, M. Goulian, T. C. Lubensky, and A. G. Yodh (2007), “Fluctuations and Rheology in Active Bacterial Suspensions,” *Phys. Rev. Lett.* **99** (14), 148302.
- Curatolo, A I, N. Zhou, Y. Zhao, C. Liu, A. Daerr, J. Tailleur, and J. Huang (2020), “Cooperative pattern formation in multi-component bacterial systems through reciprocal motility regulation,” *Nat. Phys.* **16** (11), 1152–1157.
- D’Alessandro, Joseph, Alexandre P. Solon, Yoshinori Hayakawa, Christophe Anjard, François Detcheverry, Jean-Paul Rieu, and Charlotte Rivière (2017), “Contact enhancement of locomotion in spreading cell colonies,” *Nat. Phys.* **13** (10), 999–1005.
- D’Alessio, Luca, Yariv Kafri, and Anatoli Polkovnikov (2016), “Negative mass corrections in a dissipative stochastic environment,” *J. Stat. Mech. Theory Exp.* **2016** (2), 023105.
- Daniels, Ruth, Jos Vanderleyden, and Jan Michiels (2004), “Quorum sensing and swarming migration in bacteria,” *FEMS Microbiol. Rev.* **28** (3), 261–289.
- Dean, David S (1996), “Langevin equation for the density of a system of interacting Langevin processes,” *J. Phys. A. Math. Gen.* **29** (24), L613–L617.
- Derrida, Bernard (1983), “Velocity and diffusion constant of a periodic one-dimensional hopping model,” *J. Stat. Phys.* **31** (3), 433–450.
- Derrida, Bernard, and Y. Pomeau (1982), “Classical Diffusion on a Random Chain,” *Phys. Rev. Lett.* **48** (9), 627–630.
- Deseigne, Julien, Olivier Dauchot, and Hugues Chaté (2010), “Collective Motion of Vibrated Polar Disks,” *Phys. Rev. Lett.* **105** (9), 098001.
- Di Leonardo, R, L. Angelani, D. Dell’Arciprete, G. Ruocco, V. Iebba, S. Schippa, M. P. Conte, F. Mearini, F. De Angelis, and E. Di Fabrizio (2010), “Bacterial ratchet motors,” *Proc. Natl. Acad. Sci.* **107** (21), 9541–9545.
- Digregorio, Pasquale, Demian Levis, Antonio Suma, Leticia F. Cugliandolo, Giuseppe Gonnella, and Ignacio Pagonabarraga (2018), “Full Phase Diagram of Active Brownian Disks: From Melting to Motility-Induced Phase Separation,” *Phys. Rev. Lett.* **121** (9), 098003.
- Digregorio, Pasquale, Demian Levis, Antonio Suma, Leticia F. Cugliandolo, Giuseppe Gonnella, and Ignacio Pagonabarraga (2019), “2D melting and motility induced phase separation in Active Brownian Hard Disks and Dumbbells,” in *Journal of Physics: Conference Series*, Vol. 1163 (IOP Publishing) p. 012073.
- Dinelli, Alberto, Jérémy O’Byrne, Agnese Curatolo, Yongfeng Zhao, Peter Sollich, and Julien Tailleur (2022), “Non-reciprocity across scales in active mixtures,” arXiv:2203.07757 [cond-mat.stat-mech].
- Dittrich, Florian, Thomas Speck, and Peter Virnau (2021), “Critical behavior in active lattice models of motility-induced phase separation,” *Eur. Phys. J. E* **44** (4), 53.
- Dolai, Pritha, Simon Krekels, and Christian Maes (2022), “Inducing a bound state between active particles,” *Phys. Rev. E* **105** (4), 044605.
- Duan, Yu, Benoît Mahault, Yu-qiang Ma, Xia-qing Shi, and Hugues Chaté (2021), “Breakdown of Ergodicity and Self-Averaging in Polar Flocks with Quenched Disorder,” *Phys. Rev. Lett.* **126** (17), 178001.
- Engebrecht, Joanne, and Michael Silverman (1984), “Identification of genes and gene products necessary for bacterial bioluminescence,” *Proc. Natl. Acad. Sci.* **81** (13), 4154–4158.
- Falasco, G, F. Baldovin, K. Kroy, and M. Baiesi (2016), “Mesoscopic virial equation for nonequilibrium statistical mechanics,” *New J. Phys.* **18** (9), 093043.
- Fausti, G, E. Tjhung, M. E. Cates, and C. Nardini (2021), “Capillary Interfacial Tension in Active Phase Separation,” *Phys. Rev. Lett.* **127** (6), 068001.
- Feng, Mengkai, and Zhonghuai Hou (2023), “Unraveling on kinesin acceleration in intracellular environments: A theory for active bath,” *Phys. Rev. Res.* **5** (1), 013206.
- Fily, Yaouen, Aparna Baskaran, and Michael F. Hagan (2014), “Dynamics of self-propelled particles under strong confinement,” *Soft Matter* **10** (30), 5609–5617.
- Fily, Yaouen, Aparna Baskaran, and Michael F. Hagan (2015), “Dynamics and density distribution of strongly confined noninteracting nonaligning self-propelled particles in a nonconvex boundary,” *Phys. Rev. E* **91** (1), 012125.
- Fily, Yaouen, and M. Cristina Marchetti (2012), “Athermal Phase Separation of Self-Propelled Particles with No Alignment,” *Phys. Rev. Lett.* **108** (23), 235702.
- Fisher, Daniel S (1984), “Random walks in random environments,” *Phys. Rev. A* **30** (2), 960–964.
- Fisher, Daniel S, Jürg Fröhlich, and Thomas Spencer (1984), “The Ising model in a random magnetic field,” *J. Stat. Phys.* **34** (5-6), 863–870.
- Fodor, Étienne, and Cristina Marchetti (2018), “The statistical physics of active matter: From self-catalytic colloids to living cells,” *Phys. A Stat. Mech. its Appl.* **504**, 106–120.
- Fodor, Étienne, Cesare Nardini, Michael E. Cates, Julien Tailleur, Paolo Visco, and Frédéric van Wijland (2016), “How Far from Equilibrium Is Active Matter?” *Phys. Rev. Lett.* **117** (3), 038103.
- Fruchart, Michel, Ryo Hanai, Peter B. Littlewood, and Vincenzo Vitelli (2021), “Non-reciprocal phase transitions,” *Nature* **592** (7854), 363–369.
- Fuqua, W C, S. C. Winans, and E. P. Greenberg (1994), “Quorum sensing in bacteria: the LuxR-LuxI family of cell density-responsive transcriptional regulators,” *J. Bacteriol.* **176** (2), 269–275.
- Galajda, Peter, Juan Keymer, Paul Chaikin, and Robert Austin (2007), “A Wall of Funnel Concentrates Swimming Bacteria,” *J. Bacteriol.* **189** (23), 8704–8707.
- Garcia, Simon, Edouard Hannezo, Jens Elgeti, Jean-François Joanny, Pascal Silberzan, and Nir S. Gov (2015), “Physics of active jamming during collective cellular motion in a monolayer,” *Proc. Natl. Acad. Sci.* **112** (50), 15314–15319.
- Genot, Felix, Alexandre Solon, Yariv Kafri, Christophe Ybert, Julien Tailleur, and Cecile Cottin-Bizonne (2018), “Sedimentation of self-propelled Janus colloids: polarization and pressure,” *New J. Phys.* **20** (11), 115001.
- Glaus, U (1986), “Correlations in the two-dimensional random-field Ising model,” *Phys. Rev. B* **34** (5), 3203–3211.
- Granek, Omer (2023), “Universal fluctuations of local measurement in low-dimensional systems,” arXiv:2308.08595 [cond-mat.stat-mech].
- Granek, Omer, Yongjoo Baek, Yariv Kafri, and Alexandre P. Solon (2020), “Bodies in an interacting active fluid: far-field influence of a single body and interaction between two bodies,” *J. Stat. Mech. Theory Exp.* **2020** (6), 063211.
- Granek, Omer, Yariv Kafri, and Julien Tailleur (2022), “Anomalous Transport of Tracers in Active Baths,” *Phys.*



- Rev. Lett. **129** (3), 038001.
- Hammer, Brian K, and Bonnie L. Bassler (2003), “Quorum sensing controls biofilm formation in *Vibrio cholerae*,” *Mol. Microbiol.* **50** (1), 101–104.
- Hänggi, Peter, and Peter Jung (1994), “Colored noise in dynamical systems,” *Adv. Chem. Phys.* **89**, 239–326.
- Hanna, S, W. Hess, and R. Klein (1981), “The velocity autocorrelation function of an overdamped Brownian system with hard-core interaction,” *J. Phys. A. Math. Gen.* **14** (12), L493–L498.
- Harder, J, C. Valeriani, and A. Cacciuto (2014), “Activity-induced collapse and reexpansion of rigid polymers,” *Phys. Rev. E* **90** (6), 062312.
- Hennes, Marc, Katrin Wolff, and Holger Stark (2014), “Self-Induced Polar Order of Active Brownian Particles in a Harmonic Trap,” *Phys. Rev. Lett.* **112** (23), 238104.
- Hermann, Sophie, Daniel de las Heras, and Matthias Schmidt (2019), “Non-negative Interfacial Tension in Phase-Separated Active Brownian Particles,” *Phys. Rev. Lett.* **123** (26), 268002.
- Howse, Jonathan R, Richard A. L. Jones, Anthony J. Ryan, Tim Gough, Reza Vafabakhsh, and Ramin Golestanian (2007), “Self-Motile Colloidal Particles: From Directed Propulsion to Random Walk,” *Phys. Rev. Lett.* **99** (4), 048102.
- Ilker, Efe, and Jean-François Joanny (2020), “Phase separation and nucleation in mixtures of particles with different temperatures,” *Phys. Rev. Res.* **2** (2), 023200.
- Imbrie, John Z (1984), “Lower Critical Dimension of the Random-Field Ising Model,” *Phys. Rev. Lett.* **53** (18), 1747–1750.
- Imry, Yoseph, and Shang-keng Ma (1975), “Random-Field Instability of the Ordered State of Continuous Symmetry,” *Phys. Rev. Lett.* **35** (21), 1399–1401.
- Jayaram, Ashreya, and Thomas Speck (2023), “Effective dynamics and fluctuations of a trapped probe moving in a fluid of active hard discs,” *EPL* **143** (1), 17005.
- Junot, G, G. Briand, R. Ledesma-Alonso, and O. Dauchot (2017), “Active versus Passive Hard Disks against a Membrane: Mechanical Pressure and Instability,” *Phys. Rev. Lett.* **119** (2), 028002.
- Kaiser, A, H. H. Wensink, and H Löwen (2012), “How to Capture Active Particles,” *Phys. Rev. Lett.* **108** (26), 268307.
- Kaiser, Andreas, Anton Peshkov, Andrey Sokolov, Borge ten Hagen, Hartmut Löwen, and Igor S. Aranson (2014), “Transport Powered by Bacterial Turbulence,” *Phys. Rev. Lett.* **112** (15), 158101.
- Kanazawa, Kiyoshi, Tomohiko G. Sano, Andrea Cairoli, and Adrian Baule (2020), “Loopy Lévy flights enhance tracer diffusion in active suspensions,” *Nature* **579** (7799), 364–367.
- Kardar, Mehran (2007), *Statistical Physics of Fields* (Cambridge University Press).
- Kim, Ki-Won, Yunsik Choe, and Yongjoo Baek (2023), “Generic symmetry-breaking motility in active fluids,” *arXiv:2304.01645 [cond-mat.soft]*.
- Klongvessa, Natsuda, Félix Ginot, Christophe Ybert, Cécile Cottin-Bizonne, and Mathieu Leocmach (2019), “Active glass: Ergodicity breaking dramatically affects response to self-propulsion,” *Phys. Rev. Lett.* **123** (24), 248004.
- Knežević, Miloš, Luisa E Avilés Podgurski, and Holger Stark (2021), “Oscillatory active microrheology of active suspensions,” *Sci. Rep.* **11** (1), 22706.
- Knežević, Miloš, and Holger Stark (2020), “Effective Langevin equations for a polar tracer in an active bath,” *New J. Phys.* **22** (11), 113025.
- Kourbane-Houssene, Mourtaza, Clément Erignoux, Thierry Bodineau, and Julien Tailleur (2018), “Exact Hydrodynamic Description of Active Lattice Gases,” *Phys. Rev. Lett.* **120** (26), 268003.
- Kurihara, Takashi, Msato Aridome, Heev Ayade, Irwin Zaid, and Daisuke Mizuno (2017), “Non-Gaussian limit fluctuations in active swimmer suspensions,” *Phys. Rev. E* **95** (3), 030601.
- Kurtuldu, Hüseyin, Jeffrey S. Guasto, Karl A. Johnson, and J. P. Gollub (2011), “Enhancement of biomixing by swimming algal cells in two-dimensional films,” *Proc. Natl. Acad. Sci.* **108** (26), 10391–10395.
- Kwon, Chulan, Ping Ao, and David J. Thouless (2005), “Structure of stochastic dynamics near fixed points,” *Proc. Natl. Acad. Sci.* **102** (37), 13029–13033.
- Lauersdorf, Nicholas, Thomas Kolb, Moslem Moradi, Ehssan Nazockdast, and Daphne Klotsa (2021), “Phase behavior and surface tension of soft active Brownian particles,” *Soft Matter* **17** (26), 6337–6351.
- Leptos, Kyriacos C, Jeffrey S. Guasto, J. P. Gollub, Adriana I. Pesci, and Raymond E. Goldstein (2009), “Dynamics of Enhanced Tracer Diffusion in Suspensions of Swimming Eukaryotic Microorganisms,” *Phys. Rev. Lett.* **103** (19), 198103.
- Levis, Demian, and Ludovic Berthier (2015), “From single-particle to collective effective temperatures in an active fluid of self-propelled particles,” *EPL* **111** (6), 60006.
- Li, He, and H. P. Zhang (2013), “Asymmetric gear rectifies random robot motion,” *EPL* **102** (5), 50007.
- van der Linden, Marjolein N, Lachlan C. Alexander, Dirk G. A. L. Aarts, and Olivier Dauchot (2019), “Interrupted Motility Induced Phase Separation in Aligning Active Colloids,” *Phys. Rev. Lett.* **123** (9), 098001.
- Liu, Chenli, Xiongfei Fu, Lizhong Liu, Xiaojing Ren, Carlos K.L. Chau, Sihong Li, Lu Xiang, Hualing Zeng, Guan-hua Chen, Lei-Han Tang, Peter Lenz, Xiaodong Cui, Wei Huang, Terence Hwa, and Jian-Dong Huang (2011), “Sequential Establishment of Stripe Patterns in an Expanding Cell Population,” *Science* **334** (6053), 238–241.
- Liu, Guannan, Adam Patch, Fatmagül Bahar, David Yllanes, Roy D. Welch, M. Cristina Marchetti, Shashi Thutupalli, and Joshua W. Shaevitz (2019), “Self-driven phase transitions drive *Myxococcus xanthus* fruiting body formation,” *Phys. Rev. Lett.* **122** (24), 248102.
- Maes, Christian (2020), “Fluctuating Motion in an Active Environment,” *Phys. Rev. Lett.* **125** (20), 208001.
- Maggi, Claudio, Nicoletta Gnan, Matteo Paoluzzi, Emanuela Zaccarelli, and Andrea Crisanti (2022), “Critical active dynamics is captured by a colored-noise driven field theory,” *Commun. Phys.* **5** (1), 55.
- Maggi, Claudio, Umberto Marini Bettolo Marconi, Nicoletta Gnan, and Roberto Di Leonardo (2015), “Multidimensional stationary probability distribution for interacting active particles,” *Sci. Rep.* **5** (1), 10742.
- Maggi, Claudio, Matteo Paoluzzi, Luca Angelani, and Roberto Di Leonardo (2017), “Memory-less response and violation of the fluctuation-dissipation theorem in colloids suspended in an active bath,” *Sci. Rep.* **7** (1), 17588.
- Maggi, Claudio, Matteo Paoluzzi, Andrea Crisanti, Emanuela Zaccarelli, and Nicoletta Gnan (2021), “Universality class of the motility-induced critical point in large scale off-lattice simulations of active particles,” *Soft Matter* **17** (14),

- 3807–3812.
- Malakar, Kanaya, Arghya Das, Anupam Kundu, K. Vijay Kumar, and Abhishek Dhar (2020), “Steady state of an active Brownian particle in a two-dimensional harmonic trap,” *Phys. Rev. E* **101** (2), 022610.
- Mallory, S A, A. Šarić, C. Valeriani, and A. Cacciuto (2014a), “Anomalous thermomechanical properties of a self-propelled colloidal fluid,” *Phys. Rev. E* **89** (5), 052303.
- Mallory, S A, C. Valeriani, and A. Cacciuto (2014b), “Curvature-induced activation of a passive tracer in an active bath,” *Phys. Rev. E* **90** (3), 032309.
- Marchetti, M C, J. F. Joanny, S. Ramaswamy, T. B. Liverpool, J. Prost, Madan Rao, and R. Aditi Simha (2013), “Hydrodynamics of soft active matter,” *Rev. Mod. Phys.* **85** (3), 1143–1189.
- Marini Bettolo Marconi, Umberto, Claudio Maggi, and Simone Melchionna (2016), “Pressure and surface tension of an active simple liquid: a comparison between kinetic, mechanical and free-energy based approaches,” *Soft Matter* **12** (26), 5727–5738.
- Martin, David, Jérémy O’Byrne, Michael E. Cates, Étienne Fodor, Cesare Nardini, Julien Tailleur, and Frédéric van Wijland (2021), “Statistical mechanics of active Ornstein-Uhlenbeck particles,” *Phys. Rev. E* **103** (3), 032607.
- Martin, David, Daniel Seara, Yael Avni, Michel Fruchart, and Vincenzo Vitelli (2023), “An exact model for the transition to collective motion in nonreciprocal active matter,” arXiv:2307.08251 [cond-mat.stat-mech].
- Massana-Cid, Helena, Claudio Maggi, Giacomo Frangipane, and Roberto Di Leonardo (2022), “Rectification and confinement of photokinetic bacteria in an optical feedback loop,” *Nat. Commun.* **13** (1), 2740.
- Miller, Melissa B, and Bonnie L. Bassler (2001), “Quorum Sensing in Bacteria,” *Annu. Rev. Microbiol.* **55** (1), 165–199.
- Mognetti, B M, A. Šarić, S. Angioletti-Uberti, A. Cacciuto, C. Valeriani, and D. Frenkel (2013), “Living Clusters and Crystals from Low-Density Suspensions of Active Colloids,” *Phys. Rev. Lett.* **111** (24), 245702.
- Morin, Alexandre, Nicolas Desreumaux, Jean-Baptiste Caussin, and Denis Bartolo (2017), “Distortion and destruction of colloidal flocks in disordered environments,” *Nat. Phys.* **13** (1), 63–67.
- Nardini, Cesare, Étienne Fodor, Elsen Tjhung, Frédéric van Wijland, Julien Tailleur, and Michael E. Cates (2017), “Entropy Production in Field Theories without Time-Reversal Symmetry: Quantifying the Non-Equilibrium Character of Active Matter,” *Phys. Rev. X* **7** (2), 021007.
- Nealson, Kenneth H, Terry Platt, and J. Woodland Hastings (1970), “Cellular Control of the Synthesis and Activity of the Bacterial Luminescent System,” *J. Bacteriol.* **104** (1), 313–322.
- Ni, Ran, Martien A. Cohen Stuart, and Peter G. Bolhuis (2015), “Tunable Long Range Forces Mediated by Self-Propelled Colloidal Hard Spheres,” *Phys. Rev. Lett.* **114** (1), 018302.
- Nikola, Nikolai, Alexandre P. Solon, Yariv Kafri, Mehran Kardar, Julien Tailleur, and Raphaël Voituriez (2016), “Active Particles with Soft and Curved Walls: Equation of State, Ratchets, and Instabilities,” *Phys. Rev. Lett.* **117** (9), 098001.
- O’Byrne, J, and J. Tailleur (2020), “Lamellar to Micellar Phases and Beyond: When Tactic Active Systems Admit Free Energy Functionals,” *Phys. Rev. Lett.* **125** (20), 208003.
- O’Byrne, Jérémy, Alexandre Solon, Julien Tailleur, and Yongfeng Zhao (2023), “An introduction to motility-induced phase separation,” in *Out-of-equilibrium Soft Matter: Active Fluids*, Soft Matter Series, edited by Christina Kurzthaler, Luigi Gentile, and Howard A. Stone, Chap. 4 (Royal Society of Chemistry).
- Omar, Ahmad K, Hyeonjoo Row, Stewart A. Mallory, and John F. Brady (2023), “Mechanical theory of nonequilibrium coexistence and motility-induced phase separation,” *Proc. Natl. Acad. Sci.* **120** (18), e2219900120.
- Omar, Ahmad K, Zhen-Gang Wang, and John F. Brady (2020), “Microscopic origins of the swim pressure and the anomalous surface tension of active matter,” *Phys. Rev. E* **101** (1), 012604.
- Palacci, Jeremie, Stefano Sacanna, Asher Preska Steinberg, David J. Pine, and Paul M. Chaikin (2013), “Living Crystals of Light-Activated Colloidal Surfers,” *Science* **339** (6122), 936–940.
- Paliwal, Siddharth, Vasileios Prymidis, Laura Filion, and Marjolein Dijkstra (2017), “Non-equilibrium surface tension of the vapour-liquid interface of active Lennard-Jones particles,” *J. Chem. Phys.* **147** (8), 84902.
- Paliwal, Siddharth, Jeroen Rodenburg, René van Roij, and Marjolein Dijkstra (2018), “Chemical potential in active systems: predicting phase equilibrium from bulk equations of state?” *New J. Phys.* **20** (1), 015003.
- Partridge, Benjamin, and Chiu Fan Lee (2019), “Critical Motility-Induced Phase Separation Belongs to the Ising Universality Class,” *Phys. Rev. Lett.* **123** (6), 068002.
- Peng, Zhiwei, and John F. Brady (2022), “Forced microrheology of active colloids,” *Journal of Rheology* **66** (5), 955–972.
- de Pirey, Thibaut Arnould, and Frédéric van Wijland (2023), “A run-and-tumble particle around a spherical obstacle: steady-state distribution far-from-equilibrium,” arXiv:2303.00331 [cond-mat.stat-mech].
- Potiguar, Fabricio Q, G. A. Farias, and W. P. Ferreira (2014), “Self-propelled particle transport in regular arrays of rigid asymmetric obstacles,” *Phys. Rev. E* **90** (1), 012307.
- Ramaswamy, Sriram (2010), “The Mechanics and Statistics of Active Matter,” *Annu. Rev. Condens. Matter Phys.* **1** (1), 323–345.
- Redner, Gabriel S, Aparna Baskaran, and Michael F. Hagan (2013a), “Reentrant phase behavior in active colloids with attraction,” *Phys. Rev. E* **88** (1), 12305.
- Redner, Gabriel S, Michael F. Hagan, and Aparna Baskaran (2013b), “Structure and Dynamics of a Phase-Separating Active Colloidal Fluid,” *Phys. Rev. Lett.* **110** (5), 055701.
- Reichert, Julian, Leon F Granz, and Thomas Voigtmann (2021), “Transport coefficients in dense active Brownian particle systems: mode-coupling theory and simulation results,” *Eur. Phys. J. E* **44** (3), 27.
- Reichert, Julian, and Thomas Voigtmann (2021), “Tracer dynamics in crowded active-particle suspensions,” *Soft Matter* **17** (46), 10492–10504.
- Reichhardt, C, and C. J. Olson Reichhardt (2013), “Active matter ratchets with an external drift,” *Phys. Rev. E* **88** (6), 062310.
- Ro, Sunghan, Yariv Kafri, Mehran Kardar, and Julien Tailleur (2021), “Disorder-Induced Long-Ranged Correlations in Scalar Active Matter,” *Phys. Rev. Lett.* **126** (4), 048003.
- Rodenburg, Jeroen, Siddharth Paliwal, Marjolein de Jager, Peter G. Bolhuis, Marjolein Dijkstra, and René van Roij

- (2018), “Ratchet-induced variations in bulk states of an active ideal gas,” *J. Chem. Phys.* **149** (17), 174910.
- Rohwer, Christian M, Mehran Kardar, and Matthias Krüger (2020), “Activated diffusiophoresis,” *J. Chem. Phys.* **152** (8), 084109.
- Romanczuk, P, M. Bär, W. Ebeling, B. Lindner, and L. Schimansky-Geier (2012), “Active Brownian particles,” *Eur. Phys. J. Spec. Top.* **202** (1), 1–162.
- Saha, Suropriya, Jaime Agudo-Canalejo, and Ramin Golestanian (2020), “Scalar Active Mixtures: The Nonreciprocal Cahn-Hilliard Model,” *Phys. Rev. X* **10** (4), 041009.
- Saha, Suropriya, Ramin Golestanian, and Sriram Ramaswamy (2014), “Clusters, asters, and collective oscillations in chemotactic colloids,” *Phys. Rev. E* **89** (6), 062316.
- Sandford, Cato, Alexander Y. Grosberg, and Jean-François Joanny (2017), “Pressure and flow of exponentially self-correlated active particles,” *Phys. Rev. E* **96** (5), 052605.
- Schmidt, Falko, Hana Šípová-Jungová, Mikael Käll, Alois Würger, and Giovanni Volpe (2021), “Non-equilibrium properties of an active nanoparticle in a harmonic potential,” *Nat. Commun.* **12** (1), 1902.
- Schnitzer, Mark J (1993), “Theory of continuum random walks and application to chemotaxis,” *Phys. Rev. E* **48** (4), 2553–2568.
- Sepúlveda, Néstor, Laurence Petitjean, Olivier Cochet, Erwan Grasland-Mongrain, Pascal Silberzan, and Vincent Hakim (2013), “Collective Cell Motion in an Epithelial Sheet Can Be Quantitatively Described by a Stochastic Interacting Particle Model,” *PLoS Comput. Biol.* **9** (3), e1002944.
- Sesé-Sansa, E, I. Pagonabarraga, and D. Levis (2018), “Velocity alignment promotes motility-induced phase separation,” *EPL* **124** (3), 30004.
- Shea, Jeanine, Gerhard Jung, and Friederike Schmid (2022), “Passive probe particle in an active bath: can we tell it is out of equilibrium?” *Soft Matter* **18** (36), 6965–6973.
- Shi, Xia-qing, Giordano Fausti, Hugues Chaté, Cesare Nardini, and Alexandre Solon (2020), “Self-Organized Critical Coexistence Phase in Repulsive Active Particles,” *Phys. Rev. Lett.* **125** (16), 168001.
- Shin, Jaeh, Andrey G. Cherstvy, Won Kyu Kim, and Ralf Metzler (2015), “Facilitation of polymer looping and giant polymer diffusivity in crowded solutions of active particles,” *New J. Phys.* **17** (11), 113008.
- Siebert, Jonathan Tammo, Florian Dittrich, Friederike Schmid, Kurt Binder, Thomas Speck, and Peter Virnau (2018), “Critical behavior of active Brownian particles,” *Phys. Rev. E* **98** (3), 030601.
- Sinai, Ya G (1983), “The Limiting Behavior of a One-Dimensional Random Walk in a Random Medium,” *Theory Probab. Its Appl.* **27** (2), 256–268.
- Smith, Naftali R, Pierre Le Doussal, Satya N. Majumdar, and Grégory Schehr (2022), “Exact position distribution of a harmonically confined run-and-tumble particle in two dimensions,” *Phys. Rev. E* **106** (5), 054133.
- Sokolov, Andrey, Mario M. Apodaca, Bartosz A. Grzybowski, and Igor S. Aranson (2010), “Swimming bacteria power microscopic gears,” *Proc. Natl. Acad. Sci.* **107** (3), 969–974.
- Solon, A P, M. E. Cates, and J. Tailleur (2015a), “Active brownian particles and run-and-tumble particles: A comparative study,” *Eur. Phys. J. Spec. Top.* **224** (7), 1231–1262.
- Solon, A P, Y. Fily, A. Baskaran, M. E. Cates, Y. Kafri, M. Kardar, and J. Tailleur (2015b), “Pressure is not a state function for generic active fluids,” *Nat. Phys.* **11** (8), 673–678.
- Solon, Alexandre, and Jordan M. Horowitz (2022), “On the Einstein relation between mobility and diffusion coefficient in an active bath,” *J. Phys. A Math. Theor.* **55** (18), 184002.
- Solon, Alexandre P, Joakim Stenhammar, Michael E. Cates, Yariv Kafri, and Julien Tailleur (2018a), “Generalized thermodynamics of motility-induced phase separation: phase equilibria, Laplace pressure, and change of ensembles,” *New J. Phys.* **20** (7), 075001.
- Solon, Alexandre P, Joakim Stenhammar, Michael E. Cates, Yariv Kafri, and Julien Tailleur (2018b), “Generalized thermodynamics of phase equilibria in scalar active matter,” *Phys. Rev. E* **97** (2), 020602.
- Solon, Alexandre P, Joakim Stenhammar, Raphael Wittkowski, Mehran Kardar, Yariv Kafri, Michael E. Cates, and Julien Tailleur (2015c), “Pressure and Phase Equilibria in Interacting Active Brownian Spheres,” *Phys. Rev. Lett.* **114** (19), 198301.
- Speck, Thomas (2021), “Coexistence of active Brownian disks: van der Waals theory and analytical results,” *Phys. Rev. E* **103** (1), 012607.
- Speck, Thomas (2022), “Critical behavior of active Brownian particles: Connection to field theories,” *Phys. Rev. E* **105** (6), 064601.
- Speck, Thomas, and Ashreya Jayaram (2021), “Vorticity Determines the Force on Bodies Immersed in Active Fluids,” *Phys. Rev. Lett.* **126** (13), 138002.
- Spera, Gianmarco, Charlie Duclut, Marc Durand, and Julien Tailleur (2023), “Nematic torques in scalar active matter: when fluctuations favor polar order and persistence,” arXiv:2301.02568 [cond-mat.stat-mech].
- Spohn, Herbert (1980), “Kinetic equations from Hamiltonian dynamics: Markovian limits,” *Rev. Mod. Phys.* **52** (3), 569–615.
- Stenhammar, Joakim (2021), “An introduction to motility-induced phase separation,” arXiv:2112.05024 [cond-mat.soft].
- Stenhammar, Joakim, Davide Marenduzzo, Rosalind J. Allen, and Michael E. Cates (2014), “Phase behaviour of active Brownian particles: the role of dimensionality,” *Soft Matter* **10** (10), 1489–1499.
- Stenhammar, Joakim, Raphael Wittkowski, Davide Marenduzzo, and Michael E. Cates (2015), “Activity-Induced Phase Separation and Self-Assembly in Mixtures of Active and Passive Particles,” *Phys. Rev. Lett.* **114** (1), 018301.
- Stramer, Brian, and Roberto Mayor (2017), “Mechanisms and in vivo functions of contact inhibition of locomotion,” *Nat. Rev. Mol. Cell Biol.* **18** (1), 43–55.
- Szamel, Grzegorz (2014), “Self-propelled particle in an external potential: Existence of an effective temperature,” *Phys. Rev. E* **90** (1), 012111.
- Tailleur, J, and M. E. Cates (2008), “Statistical Mechanics of Interacting Run-and-Tumble Bacteria,” *Phys. Rev. Lett.* **100** (21), 218103.
- Tailleur, J, and M. E. Cates (2009), “Sedimentation, trapping, and rectification of dilute bacteria,” *EPL* **86** (6), 60002.
- Tailleur, Julien, Gerhard Gompper, M. Cristina Marchetti, Julia M. Yeomans, and Christophe Salomon, Eds. (2022), *Active Matter and Nonequilibrium Statistical Physics: Lecture Notes of the Les Houches Summer School: Volume 112, September 2018*, Vol. 112 (Oxford University Press).
- Takaha, Yuki, and Daiki Nishiguchi (2023), “Quasi-two-dimensional bacterial swimming around pillars: Enhanced

- trapping efficiency and curvature dependence,” *Phys. Rev. E* **107** (1), 014602.
- Takatori, S C, and J. F. Brady (2015), “Towards a thermodynamics of active matter,” *Phys. Rev. E* **91** (3), 032117.
- Takatori, S C, W. Yan, and J. F. Brady (2014), “Swim Pressure: Stress Generation in Active Matter,” *Phys. Rev. Lett.* **113** (2), 028103.
- Takatori, Sho C, Raf De Dier, Jan Vermant, and John F. Brady (2016), “Acoustic trapping of active matter,” *Nat. Commun.* **7** (1), 10694.
- Theurkauff, I, C. Cottin-Bizonne, J. Palacci, C. Ybert, and L. Bocquet (2012), “Dynamic Clustering in Active Colloidal Suspensions with Chemical Signaling,” *Phys. Rev. Lett.* **108** (26), 268303.
- Thiffeault, Jean-Luc (2015), “Distribution of particle displacements due to swimming microorganisms,” *Phys. Rev. E* **92** (2), 023023.
- Thompson, A G, J. Tailleur, M. E. Cates, and R. A. Blythe (2011), “Lattice models of nonequilibrium bacterial dynamics,” *J. Stat. Mech. Theory Exp.* **2011** (02), P02029.
- Thutupalli, Shashi, Ralf Seemann, and Stephan Herminghaus (2011), “Swarming behavior of simple model squirmers,” *New J. Phys.* **13** (7), 073021.
- Tjhung, Elsen, Cesare Nardini, and Michael E. Cates (2018), “Cluster Phases and Bubbly Phase Separation in Active Fluids: Reversal of the Ostwald Process,” *Phys. Rev. X* **8** (3), 031080.
- Toner, John, Nicholas Guttenberg, and Yuhai Tu (2018), “Hydrodynamic theory of flocking in the presence of quenched disorder,” *Phys. Rev. E* **98** (6), 062604.
- Toner, John, Yuhai Tu, and Sriram Ramaswamy (2005), “Hydrodynamics and phases of flocks,” *Annals of Physics* **318** (1), 170–244.
- Tsou, Amy M, and Jun Zhu (2010), “Quorum Sensing Negatively Regulates Hemolysin Transcriptionally and Post-translationally in *Vibrio cholerae*,” *Infect. Immun.* **78** (1), 461–467.
- Verma, Subhash, and Tim Miyashiro (2013), “Quorum Sensing in the Squid-*Vibrio* Symbiosis,” *Int. J. Mol. Sci.* **14** (8), 16386–16401.
- Vicsek, Tamás, András Czirók, Eshel Ben-Jacob, Inon Cohen, and Ofer Shochet (1995), “Novel Type of Phase Transition in a System of Self-Driven Particles,” *Phys. Rev. Lett.* **75** (6), 1226–1229.
- Weber, Simon N, Christoph A. Weber, and Erwin Frey (2016), “Binary Mixtures of Particles with Different Diffusivities Demix,” *Phys. Rev. Lett.* **116** (5), 058301.
- Whitelam, Stephen, Katherine Klymko, and Dibyendu Mandal (2018), “Phase separation and large deviations of lattice active matter,” *J. Chem. Phys.* **148** (15).
- Winkler, Roland G, Adam Wysocki, and Gerhard Gompper (2015), “Virial pressure in systems of spherical active Brownian particles,” *Soft Matter* **11** (33), 6680–6691.
- Wittkowski, Raphael, Joakim Stenhammar, and Michael E. Cates (2017), “Nonequilibrium dynamics of mixtures of active and passive colloidal particles,” *New J. Phys.* **19** (10), 105003.
- Wittkowski, Raphael, Adriano Tiribocchi, Joakim Stenhammar, Rosalind J. Allen, Davide Marenduzzo, and Michael E. Cates (2014), “Scalar  $\phi^4$  field theory for active-particle phase separation,” *Nat. Commun.* **5** (1), 4351.
- Wittmann, René, Claudio Maggi, A. Sharma, A. Scacchi, Joseph M. Brader, and U. Marini Bettolo Marconi (2017a), “Effective equilibrium states in the colored-noise model for active matter I. Pairwise forces in the Fox and unified colored noise approximations,” *J. Stat. Mech. Theory Exp.* **2017** (11), 113207.
- Wittmann, René, U. Marini Bettolo Marconi, C. Maggi, and J. M. Brader (2017b), “Effective equilibrium states in the colored-noise model for active matter II. A unified framework for phase equilibria, structure and mechanical properties,” *J. Stat. Mech. Theory Exp.* **2017** (11), 113208.
- Wuillez, Eric, Yariv Kafri, and Nir S. Gov (2020a), “Active Trap Model,” *Phys. Rev. Lett.* **124** (11), 118002.
- Wuillez, Eric, Yariv Kafri, and Vivien Lecomte (2020b), “Non-local stationary probability distributions and escape rates for an active Ornstein–Uhlenbeck particle,” *J. Stat. Mech. Theory Exp.* **2020** (6), 063204.
- Wu, Xiao-Lun, and Albert Libchaber (2000), “Particle Diffusion in a Quasi-Two-Dimensional Bacterial Bath,” *Phys. Rev. Lett.* **84** (13), 3017–3020.
- Wysocki, Adam, and Heiko Rieger (2020), “Capillary Action in Scalar Active Matter,” *Phys. Rev. Lett.* **124** (4), 048001.
- Wysocki, Adam, Roland G. Winkler, and Gerhard Gompper (2014), “Cooperative motion of active Brownian spheres in three-dimensional dense suspensions,” *EPL* **105** (4), 48004.
- Wysocki, Adam, Roland G. Winkler, and Gerhard Gompper (2016), “Propagating interfaces in mixtures of active and passive Brownian particles,” *New J. Phys.* **18** (12), 123030.
- Yan, Wen, and John F. Brady (2015), “The force on a boundary in active matter,” *J. Fluid Mech.* **785**, R1.
- Yan, Wen, and John F. Brady (2018), “The curved kinetic boundary layer of active matter,” *Soft Matter* **14** (2), 279–290.
- Yang, Xingbo, M. Lisa Manning, and M. Cristina Marchetti (2014), “Aggregation and segregation of confined active particles,” *Soft Matter* **10** (34), 6477–6484.
- You, Zhihong, Aparna Baskaran, and M. Cristina Marchetti (2020), “Nonreciprocity as a generic route to traveling states,” *Proc. Natl. Acad. Sci.* **117** (33), 19767–19772.
- Zaeifi Yamchi, Mahdi, and Ali Najji (2017), “Effective interactions between inclusions in an active bath,” *J. Chem. Phys.* **147** (19), 194901.
- Zaid, Irwin M, Jörn Dunkel, and Julia M. Yeomans (2011), “Lévy fluctuations and mixing in dilute suspensions of algae and bacteria,” *J. R. Soc. Interface* **8** (62), 1314–1331.
- Zakine, R, Y. Zhao, M. Knežević, A. Daerr, Y. Kafri, J. Tailleur, and F. van Wijland (2020), “Surface Tensions between Active Fluids and Solid Interfaces: Bare vs Dressed,” *Phys. Rev. Lett.* **124** (24), 248003.
- Zhang, Jie, Ricard Alert, Jing Yan, Ned S. Wingreen, and Steve Granick (2021), “Active phase separation by turning towards regions of higher density,” *Nat. Phys.* **17** (8), 961–967.
- Zhao, Hongbo, Andrej Košmrlj, and Sujit S. Datta (2023), “Chemotactic motility-induced phase separation,” *Phys. Rev. Lett.* **131**, 118301.